SPLITTING SUPERSONIC NOZZLE FLOW INTO SEPARATE JETS BY OVEREXPANSION INTO A MULTILOBED DIVERGENT NOZZLE

by Ronald G. Huff and Donald E. Groesbeck

Lewis Research Center
Cleveland, Ohio 44135

NATIONAL AERONAUTICS AND SPACE ADMINISTRATION • WASHINGTON, D. C. • MARCH 1972

1. Report No.	2. Government Accession No.	3. Recipient's Catalog No.
NASA TN D-6667		

4. Title and Subtitle: SPLITTING SUPERSONIC NOZZLE FLOW INTO SEPARATE JETS BY OVEREXPANSION INTO A MULTILOBED DIVERGENT NOZZLE

5. Report Date: March 1972

6. Performing Organization Code:

7. Author(s): Ronald G. Huff and Donald E. Groesbeck

8. Performing Organization Report No.: E-6640

9. Performing Organization Name and Address:
Lewis Research Center
National Aeronautics and Space Administration
Cleveland, Ohio 44135

10. Work Unit No.: 132-80

11. Contract or Grant No.:

12. Sponsoring Agency Name and Address:
National Aeronautics and Space Administration
Washington, D.C. 20546

13. Type of Report and Period Covered: Technical Note

14. Sponsoring Agency Code:

15. Supplementary Notes:

16. Abstract

Air flowing from a convergent nozzle at pressure ratios greater than 2.5 has been split into eight separate jets by overexpansion of the flow into a divergent, eight-lobed passage. The splitting of the flow is accompanied by a decrease in the nozzle axial centerline Mach number. This in part is due to the radial inflow of secondary air between the lobes toward the nozzle centerline. Each of the smaller jets is partially split after it leaves the end of the divergent lobed section of the nozzle, thus creating a velocity profile having 16 peaks. At a pressure ratio of 3.5 the flow decelerates to Mach 1 in three convergent nozzle throat diameters. Convergent nozzle flow normally requires 12 diameters to reach Mach 1. The nozzle has a sound attenuation of 12 decibels with a thrust loss of 9 percent for the best configuration tested.

17. Key Words (Suggested by Author(s))		18. Distribution Statement
Jet noise	Overexpanded jet	Unclassified - unlimited
Jet mixing	Supersonic flow	
Noise suppressor		
Mixing nozzle		

19. Security Classif. (of this report)	20. Security Classif. (of this page)	21. No. of Pages	22. Price*
Unclassified	Unclassified	55	$3.00

* For sale by the National Technical Information Service, Springfield, Virginia 22151

SPLITTING SUPERSONIC NOZZLE FLOW INTO SEPARATE JETS BY OVEREXPANSION INTO A MULTILOBED DIVERGENT NOZZLE

by Ronald G. Huff and Donald E. Groesbeck

Lewis Research Center

SUMMARY

A mixing nozzle designed to promote jet mixing and rapid decay of the jet maximum velocity has been tested using ambient temperature air. The nozzle uses the unorthodox approach of overexpanding the flow from the circular convergent nozzle throat into eight separate jets positioned around the nozzle exit and diverging from the jet centerline at a 15° angle. As the flow is being turned secondary air is channeled between the eight expanding jets. The secondary air causes the already overexpanded supersonic flow along the lobes to decelerate through shock waves and results in an extremely rapid decrease of the nozzle centerline Mach number to 0.4. Each of the eight jets divide again to form a velocity profile having 16 peaks. At a nozzle pressure ratio of 3.5 the jet has decelerated to Mach 1 in three primary nozzle diameters. The nozzle exhibits sound suppression on the order of 12 decibels with a thrust loss of 9 percent for the best configuration tested.

INTRODUCTION

As the weight, velocity, and size of jet aircraft increases, the engine size or operating pressure ratio must be increased in order to overcome increases in drag. Increasing either the size for a given thermodynamic cycle of jet engines or the jet velocity results in an increase of jet noise (Lighthill, ref. 1).

The primary factor in jet noise generation is the jet velocity. Work by Greatrex (ref. 2), showed that reductions in sound levels could be obtained by using a multilobed mixing nozzle. This increased the initial surface area of the jet exposed to the surrounding air, promoted the initial mixing, and shortened the length of the core region. A summary illustrating several types of mixing nozzles is given in reference 3. These mixing nozzles attempt to decrease the jet velocity in a shorter distance by increasing the exposed surface area of the jet to the surrounding low-energy air. Interference

between adjacent jets also plays a part in the sound attenuation obtained using these nozzles.

The purpose of this report is to introduce a new type of mixing nozzle, show its principle of operation, and provide thrust loss data along with limited acoustic measurements to illustrate the possible magnitude of the noise suppression when compared with a plain conical nozzle.

Figure 1 presents pictures of the divergent lobed nozzle. Figure 1(a) is a view of the nozzle looking downstream. Figure 1(b) is a rear view of the nozzle looking directly upstream along the jet axis. The nozzle consist of two basic parts (fig. 2): first, the convergent primary nozzle and, second, the divergent lobed section attached at the primary nozzle exit. All symbols used in this report are defined in appendix A.

Tests on the nozzle shown in figure 1 were conducted as a part of a jet noise reduction program in a cold flow air facility located at the NASA Lewis Research Center. The convergent primary nozzle throat diameter was 7.62 centimeters. The total temperature of the air ranged from 280 to 285 K. The ratio of the nozzle total to atmospheric pressure was varied from 1.5 to 4.0. Thrust, jet total and static pressure profiles, primary plate static pressures, and ejector secondary mass flow rate were measured. Noise measurements at the peak jet noise location were made during tests of the nozzle. Measurements of the primary nozzle noise without the divergent section attached were made for comparison purposes.

NOZZLE DESCRIPTION AND OPERATION

The complete nozzle assembly consists of three main parts (figs. 2 and 3): (1) the primary nozzle, (2) divergent lobed section, and (3) the ejector shroud. Figure 2 is a cross sectional drawing, and figure 3 is a photograph of an exploded view of the nozzle.

The divergent lobed section of the nozzle consists of eight primary plates, rectangular in plan form with one short side attached at the primary nozzle exit (figs. 1 and 2). The primary plates are diverged from the nozzle axial centerline at a 15° angle. Attached to the primary plates are side plates. A portion of the space between adjacent primary plates and the primary nozzle exit is sealed by placing V-shaped gutter plates between the primary plates and the primary nozzle exit. A step existed between the throat of the primary nozzle and the primary plates.

In operation, the primary nozzle flow expands from the primary nozzle exit into the channel formed by the primary plates and the V-shaped gutter plates. This expansion is increased by the pumping action of the jet on the sealed base cavity formed by the step between the primary nozzle throat and the primary plates. The pumping action of the flow on the sealed base cavity creates a base pressure which is lower than the ambient air pressure causing the flow to overexpand. The flow impinges on the primary

plates and at the same time is distributed among the primary plates by the splitting action of the apex of the V-shaped gutter plates on the expanding flow. The impingement of the flow on the primary plates sets up a shock system in the divergent lobed section of the nozzle. At the centerline the shocks and their reflected shocks cause the flow along the centerline to decelerate rapidly.

At the downstream end of the gutter plates secondary air from the ejector (fig. 2) flows toward the nozzle centerline because the static pressure of the jet is lower than that of the secondary ejector air. The flow along the centerline sees an adverse pressure gradient because of this inflow and continues to decelerate subsonically. As this action occurs, the flow is diverted to flow along the primary plates. This action creates a separate jet for each primary plate. Hence, in the test eight jets result.

As the separated jet proceeds along the primary plate, it is shielded from the secondary flow by the primary side plates (fig. 2). Between the end of the gutter plates and the downstream end of the primary plates, the ejector secondary flow penetrates the primary jet flow causing each jet to form a velocity profile which has two peaks. This phenomenon is not clearly understood at this writing. This amounts to an additional splitting of the jet flow and results in a velocity profile having 16 peaks.

Thus, the primary nozzle flow has been divided into a 16-peak velocity profile exposing more of the high velocity flow to the low-energy secondary and ambient air. This promotes mixing and a more rapid decay in the jet velocity than can be obtained with a plain convergent nozzle jet.

APPARATUS

Nozzle Configurations

The nozzle configurations are shown in figure 2 along with the important dimensions. The addition of the letter "E" to the configuration code indicates that the ejector shroud had been installed. The addition of the letter "S" to the configuration code indicates that the secondary ejector flow was measured, and the letter "V" refers to the V-shaped gutter plate. The numbers following the letters are the length in primary nozzle throat diameters of the piece referred to by the preceding letter. Hence the code used in this report will appear as follows:

$$\text{Configuration number} - V\left(\begin{array}{c}\text{Length of V-shaped}\\ \text{gutter plate in noz-}\\ \text{zle throat diameters}\end{array}\right) - E\left(\begin{array}{c}\text{Length of ejector}\\ \text{in nozzle throat}\\ \text{diameter}\end{array}\right) - S$$

The primary difference between configurations 1 - V(1.33) and 2 - V(0.75) was the length of the gutter plates L_v. Another difference between configurations 1 - V(1.33) and 2 - V(0.75) was the length of the primary plates L_p.

Different ejector shroud lengths L_e were used for configurations 1 - V(1.33) - E(4) and 2 - V(0.75) - E(2). In all other respects configurations 1 - V(1.33) and 2 - V(0.75) were the same. The divergence angle of the primary plates was 15^o. The width of the primary plates was 2.54 centimeters. The height of the primary side plates was 0.5 centimeter. The primary nozzle throat diameter was 7.62 centimeters. And the height of the step between the nozzle throat diameter and the primary plate centerline at the primary nozzle exit was 0.32 centimeter.

An exploded view of the nozzle is shown in figure 3. The divergent portion of the nozzle fit on the convergent primary nozzle so that the inner portion or apex of the V-shaped gutter plates would just rest on an imaginary cylinder having a diameter equal to the primary nozzle throat diameter and concentric with the nozzle axial centerline (fig. 1(b)). The apex of the V-shaped gutter plate was parallel with the nozzle centerline.

The ejector used on configuration 2 - V(0.75) - E(2) was equal in length to twice the primary nozzle diameter D_t. The ejector shroud inside diameter was also equal to $2D_t$. The ejector fit over the primary plate support ring shown in figure 3 and was positioned so that the start of its constant area section after the entrance bellmouth was in the plane of the primary nozzle throat (see fig. 2).

Figure 4 shows photographic details of configuration 2 - V(0.75) - E(2). Figure 4(a) shows the passage through which ejector secondary air flows before mixing with the primary air flow. The secondary air is split as it flows into the ejector by the blockage created by the primary plates and is forced to flow into the V-shaped passage formed by the gutter plates. All the secondary flow was ducted into the gutter plates for configuration 1 - V(1.33) - E(4) since the primary plates extended to the inside diameter of the ejector shroud. To modify this situation, the primary plates were cut off just short of the ejector shroud for configuration 2 - V(0.75) - E(2) as shown in figure 4(b). The length of the gutter plate was also shortened resulting in more exposure of the primary jet to the secondary flow. Figure 4(c) is an oblique rear view of configuration 2 - V(0.75) - E(2) and shows the extent of the secondary flow area compared with the primary nozzle size. The reader's attention is drawn to the apex of the gutter plates. This is arranged so that, when the flow is not turned on to the primary plates, it will flow out of the nozzle in the axial direction while touching only the apex of the gutter plates. This condition exists when the base cavity is not sealed.

With the primary nozzle flow separated from the primary and gutter plates, the forces on these plates are greatly reduced. This would allow free movement of these plates to form, for instance, a convergent-divergent nozzle for supersonic jet exit velocity or a simple duct for the flow from the primary nozzle for subsonic or low supersonic

jet velocities. Such a capability is considered important for supersonic aircraft application.

Facility Description and Instrumentation

Cold air (280 to 285 K) was supplied to the test facility from a central air supply system. The facility piping system is shown schematically in figure 5. Air was piped to the test nozzle through an overhead pipe in which the air temperature was measured using an ISA type K thermocouple. Located in the overhead pipe was a mass flow rate measuring orifice plate, having flange pressure taps. The upstream pressure was read using a bourdon type pressure gage, and the difference between the orifice tap pressures was read on a U-tube mercury manometer board. This instrumentation yields the information needed to calculate the mass flow rate through the nozzle. Air from the orifice passed through a remotely operated butterfly valve used to control the nozzle inlet total pressure and mass flow rate.

Just downstream of the valve the flow was split and ducted into two smaller pipes as shown in figure 5 (section A-A). The flow passed through the 180^{o} elbows, through the flexible connections and then entered the pipe which supplied the test configuration with air. This pipe was suspended from the overhead pipe by cables. Since the pipe was not restrained in its horizontal movement, the thrust of the test nozzle can be measured by placing a strain gage load cell in line with the pipe centerline and restraining the load cell at one end as shown in figure 5. Care was exercised so that the pipe on which the test nozzles were installed was positioned so that the flex joints centerlines were alined perpendicular with the nozzle air supply pipe. If this had not been done, an error in the thrust measurements would have resulted because of the air supply piping pressure forces having a force component along the jet centerline.

The output of the load cell circuitry was measured using a digital voltmeter. The load cell was calibrated using a dead weight tester and was linear.

The nozzle total pressure was measured using a single total-pressure probe located on the centerline of the air supply pipe just upstream of the converging portion of the primary nozzle (fig. 5). A precision bourdon tube pressure gage was used to read the pressure.

With the ejector installed the secondary air mass flow rate was measured by installing a large box over the inlet to the ejector (fig. 6). Bellmouths were located on the top, bottom, and two sides of the box. Figure 6 shows the bellmouths located on the box and the air supply pipe entering the box from the left. The direction of the air jet flow was from left to right. Four static pressure taps were located at the throat of each bellmouth. In addition, the box inner-wall static pressures were measured. These

were connected to water manometer boards using atmospheric air pressure as their reference. A barometer measured atmospheric pressure. The manometer board pressures along with atmospheric air temperature and pressure are sufficient to determine the mass flow rate of air through the bellmouths and hence the secondary mass flow rate through the ejector.

A pitot-static tube was used to survey the jet total and static pressures. The pitot-static tube was remotely translatable in the horizontal and vertical direction perpendicular to the jet axial centerline. The pitot-static tube was removable, and, when surveys closer to the nozzle than 4 primary nozzle diameters ($x/D_t = 4$) were required, another pitot-static tube was installed that could be extended upstream as far as the primary nozzle throat station.

The pitot total and static pressures were converted to electrical signals by strain-gage absolute pressure transducers. The output of their signal conditioning equipment was connected to the y-axes of an x-y-y' plotter which could record two channels of information on the ordinate. The x-axis of the plotter was used to record the horizontal traversing position of the pitot-static tube. In this way the total and static pressures in the jet were plotted as functions of the distance across the jet. Using the data from these plots, the jet Mach number was calculated.

Static pressure taps were installed on the jet side surface of one of the primary plates as well as in the primary nozzle base. These were connected to mercury manometer boards, which used atmospheric pressure for reference. These were read and recorded manually.

The sound pressure levels were measured using a hand held sound meter (see fig. 7(a)) using the C-weighted compensating filter network. The C-weighted network has a frequency response that is flat within 4 decibels from 30 to 10 000 hertz. The meter was held at approximately the elevation of the nozzle centerline as shown in figure 7(a). A sound level survey was taken around the jet at 15°, 30°, 45°, and 60° from the jet axis and at a constant radial distance of 6 meters to determine the maximum sound pressure level. This generally occurred at 30° from the jet centerline, and in some cases occurred at the 45° location. Figure 7(a) shows the sound field looking in a direction which is approximately 30° off the jet centerline. The sound meter is being held at the 30° 6-meter location. Figure 7(b) shows the sound field looking from the 20° angular location at the nozzle exit. These photographs show that the sound field had many reflecting surfaces thus making it poor for acoustic measurements. However, the gross sound pressure levels measured were used for relative comparison purposes and therefore are considered to be of value even though their absolute values are questionable. Further discussion concerning these measurements and their accuracy is presented in the section RESULTS AND DISCUSSION.

TEST PROCEDURE

The test configuration was installed so that a horizontal pitot-static tube survey normal to the jet axis was centered on two diametrically opposite primary plates. The total pressure of the nozzle was set so that any one of several nominal ratios of nozzle total to atmospheric pressure resulted. The jet pitot tube total and static pressures were plotted on graph paper by traversing the pitot-static tube across the jet. The primary plate and primary nozzle base (or step) pressures were read from the mercury manometer boards and recorded manually. The output of the thrust load cell was recorded along with the barometer reading, air supply temperature, and orifice upstream pressure. The orifice pressure differences were read from the U-tube mercury manometer board and recorded. This procedure was carried out over a range of nozzle pressure ratios of 1.5 to 4.0.

The pitot-static tube was then traversed out of the jet wake to avoid errors in noise measurements due to its presence in the jet stream creating added noise. Noise measurements were taken over the nozzle pressure range using the hand held sound pressure level meter set for a C-weighting curve response at varying angular locations from the jet axis. A check was made of the noise meter readings to insure that the maximum lobe noise was measured. A check was also made of the sound pressure level using the flat frequency response (30 to 20 000 Hz) curve to determine if a significant amount of the noise existed at higher frequencies. An increase on the order of 3 decibels was noted for both the plain convergent nozzle and the divergent multilobed nozzles.

This procedure was repeated, with the exception of the noise and thrust measurements, over the range of nozzle pressure ratios with the secondary flow box installed. The bellmouth static pressure along with an inside box static pressure were measured using water manometer boards. The agreement among the bellmouth static pressure and the box static pressures was excellent, and so little scatter was found that only an average value was recorded.

Nozzle total pressures of 50.3, 101, 143, 199, and 291 kilonewtons per square meter (7.3, 14.7, 20.8, 28.8, 35.5, and 42.3 psig) were used for each configuration; there were some variations in pressure ratio due to changes in atmospheric pressure. The air total temperature ranged from 280 to 285 K. The configurations tested were as follows (see APPARATUS, Nozzle Configurations): 1 - V(1.33), 1 - V(1.33) - E(4), 1 - V(1.33) - E(4) - S, 2- V(0.75), 2 - V(0.75) - E(2), and 2 - V(0.75) - E(2) - S.

DATA REDUCTION

The pressures measured using manometer boards referenced to atmospheric pressure were reduced as follows:

The difference in the level between the reference manometer tube fluid height and the height of the fluid in the manometer tube measuring the unknown pressure was computed. This value was added algebraically to the barometer reading resulting in the absolute pressure value in terms of height of manometer fluid. Manometer board temperature did not vary significantly so that density corrections were not needed.

The mass flow rate through the orifice was calculated using the method and equation given for flange tap orifice plates in reference 4. The equation is

$$W_p = KA_{or}Y\sqrt{2\rho(p_1 - p_2)}$$

where K is the orifice coefficient taken equal to 0.672, A_{or} is the orifice area and equals 0.00818 square meter, Y is the expansion coefficient and equals 0.995 over operating range, ρ is the upstream density of air (kg/m^3), p_1 is the upstream flange tap pressure (N/m^2), and p_2 is the downstream flange tap pressure.

The secondary mass flow rate through each bellmouth located in the secondary flow measuring box was calculated assuming isentropic, adiabatic flow of an ideal gas having a total pressure equal to atmospheric pressure. The equation used from continuity consideration was

$$W_b = \frac{pM_b}{\sqrt{\frac{t}{T}}}\sqrt{\frac{\gamma A_b^2}{RT}}$$

where p is the measured bellmouth static pressure (N/m^2), M_b is the bellmouth Mach number calculated from the ratio of bellmouth static to atmospheric pressure and using isentropic flow equations, t/T is the ratio of static to total temperature from isentropic flow equations, γ is the ratio of specific heats for air, A_b is the area of the bellmouth throat (m^2), R is the gas constant for air (N-m/kg-K), and T is the atmospheric air temperature (K).

The total secondary flow was calculated by multiplying the flow through one bellmouth by 4 to account for the four bellmouths installed in the measuring box sides; that is, $W_s = 4W_b$.

The ideal conical nozzle net thrust was calculated from the following equation:

$$F_n = W_{pt}V_{pt} + A_{pt}(p_{pt} - p_o)$$

where W_{pt} is the primary mass flow rate (kg/sec) calculated using the conditions at the primary throat (for subcritical pressure ratios, the throat static pressure was assumed

to equal the atmospheric pressure), V_{pt} is the primary flow velocity at the throat station (m/sec), A_{pt} is the throat area of the primary nozzle (m^2), p_{pt} is the static pressure at the throat station in the primary nozzle (N/m^2), and p_o is the atmospheric pressure (N/m^2).

RESULTS AND DISCUSSION

Splitting of Flow into Separate Jets

A horizontal total-pressure survey normal to the jet axis was taken across two opposite primary plates through their centerlines at various axial distances downstream. These surveys yield the information needed to define the jet flow pattern. Traces were taken using the pitot tube and traversing mechanism as discussed earlier in this report. The pitot-static total pressure was machine plotted as a function of horizontal distance across the jet for various axial locations for configuration 1 - V(1.33). Plots at selected axial distances are shown in figure 8 to show the division of the jet into a separate jet for each plate and finally into a jet total-pressure profile having two peaks for each primary plate. A more detailed set of pitot total- and static-pressure profiles giving the profiles at a greater number of axial locations and over a pressure ratio range of 2.5 to 3.5 is included in appendix B. It is important to realize that the machine plots yield the total pressure that the pitot tube sees and that, if the Mach number of the streamline approaching the pitot tube is greater than one, a bow shock will position itself in front of the pitot tube. Because of this shock and the resulting total-pressure loss, the pitot-static tube measures the total pressure downstream of the shock, and it is this value that is recorded on the x-y-y' plotter. No corrections for this shock loss has been made in the machine plots presented in figure 8 or in appendix B.

Figure 8(a) is the jet total pressure profile at the primary nozzle exit or throat station $x/D_t = 0$. The total pressure set for the profiles shown was 345 kilonewtons per square meter, $P_N/p_o = 3.52$. The nozzle total pressure read by the pitot-static tube from figure 8(a) is 341 kilonewtons per square meter. At the end of the gutter plates (an axial distance of $x/D_t = 1.33$, fig. 8(b)), the pitot-static total-pressure profile shows that the jet has been divided among the primary plates. The nozzle centerline Mach number at this point is 0.89, and the Mach number of the primary plate jets is 1.61. Injecting a small amount of water at the end of the gutter plates visually showed that the secondary flow was being pulled toward the jet centerline in the radial direction. This indicated a complete division of the jet among the eight primary plates.

Figure 8(c) shows the pitot total pressure profile at an axial location just downstream of the end of the primary plates. At this point the centerline flow has reached

Mach 0.43 while the outer jets peak value is Mach 1.43. The profile at the centerline has started to fill in at this $x/D_t = 1.85$ and at the same time the jets moving along the primary plates are starting to divide in the region of 4 centimeters off the axial centerline. Figure 8(d) shows that these conditions continue as the jet proceeds downstream to an $x/D_t = 3.00$. At this axial distance the centerline Mach number has increased to 0.83 because of mixing of the inner jets while the outer jets have a Mach number of 1.04 (identified as the sonic point). When the jet reaches an $x/D_t = 4.00$ (fig. 8(e)), the Mach number of the jet is less than 1, and the centerline Mach number has increased to 0.92.

The conclusion which is drawn from the data presented in figure 8 is that the jet has been split into eight separate jets and that these jets are in turn partially divided to form a velocity profile that has 16 peaks. The energy in these jets is dissipated by mixing with the surrounding air, and, for these data taken at a nozzle pressure ratio of 3.52, the jet Mach number is reduced to subsonic values in 4 primary nozzle diameters. The sonic point in a plain conical nozzle jet is located at 11.6 primary nozzle diameters for the nozzle pressure ratio of 3.52 (ref. 5).

Primary Plate Static Pressures

The primary plate axial static-pressure distribution is shown in figure 9 over the test nozzle pressure ratios range for configurations 1 - V(1.33), 1 - V(1.33) - E(4), 2 - V(0.75), and 2 - V(0.75) - E(2). (See APPARATUS, Nozzle Configurations section and fig. 2 for configuration coding and dimensions.) The pressures are presented in pressure coefficient form (primary plate surface static pressure minus atmospheric pressure divided by the primary nozzle total pressure) plotted against the plate distance in terms of primary nozzle diameters measured from the primary nozzle exit station. The negative pressure coefficients indicate that the plate pressures are lower than atmospheric pressure. Large negative values of the coefficient indicate attachment of the flow to the primary plate. All configurations show definite sustained attachment of the flow to the primary plates in the nozzle pressure ratio range of 3.0 to 4.0 and at least attachment and then separation at a pressure ratio of 2.5. Partial attachment appeared to exist at a pressure ratio of 1.5 to 2 for configurations 1 - V(1.33) - E(4) and 2 - V(0.75). However, it was observed during the tests that at times the flow attached to two or three of the plates while at low pressure ratios and that the attachment could be moved from plate to plate by restricting the secondary flow by placing a hand over the gutter plate region.

The sharp increase in the plate static pressure observed at pressure ratios above 2.5 in the $x/D_t = 0$ to 0.2 region is caused by the flow overexpanding into the base cavity and being turned at the primary plate thus creating an oblique shock.

The sharp increase of the primary plate static pressure in the region near the end of the gutter plates for all configurations is caused by reflected shocks and the adjustment of the low jet static pressure existing on the primary plates and in the jet to the relative high static pressure of the secondary air. This pressure difference forces secondary air into the primary jet. Shocks result and the static pressure of the jet begins to adjust itself to the secondary static pressure.

As should be expected, the length of the gutter plate determined the location of the strong shock and inflow of secondary flow toward the jet centerline. Configuration 1 - V(1.33) (fig. 9(a)) and configuration 2 - V(0.75) (fig. 9(c)) illustrate this.

In the case of configuration 1 - V(1.33) - E(4) (fig. 9(b)), the addition of the ejector appears to have increased the attachment of the jets to the primary plate at a pressure ratio of 2.5. The ejector appears to have in effect increased the nozzle pressure ratio for configuration 1 - V(1.33) by lowering the pressure that the flow sees as it leaves the nozzle. The ejector for this configuration was 4 primary nozzle diameters long and had been expected to pump better than the ejector used on configuration 2 - V(0.75) - E(2) which was 2 nozzle diameters long.

Adding an ejector to configuration 2 - V(0.75) had less effect on the primary plate static pressures than was observed for configuration 1 - V(1.33) - E(4). This was observed in the plate static pressure observed at the end of the gutter plates. The addition of the ejector to configuration 2 - V(0.75) by comparison of the static pressures shown in figures 9(c) and (d) at $x/D_t = 1.0$ and 1.17, respectively, show that the ejector lowered the static pressure at the end of the gutter plates.

Axial Pitot-Tube Static and Total Pressures

From the pitot-static tube surveys made over a range of axial distances x (a representative portion is shown in appendix B), the centerline static pressure and pitot-tube total pressure were determined. Using the ratio of the static and the pitot-tube total pressure, a total pressure upstream of the pitot-tube bow shock was determined using the tables given in reference 6 by correcting the pitot tube total pressure for the normal shock pressure loss.

The corrected total pressures and static pressures shown as ratios of the nozzle total pressure appear in figure 10 as a function of axial distance.

Also the primary plate total pressure distributions are shown. They were corrected in the same manner as the centerline values but in this case the primary plate static pressures were used in place of the pitot-tube static pressure. The data are shown for configuration 1 - V(1.33) at nozzle pressure ratios from 2.47 to 3.52.

The centerline static pressures decrease initially with axial distance while the centerline total pressure remained constant. This indicates an initial supersonic expansion

on the centerline. At the point where the static pressure starts to increase, the flow experiences a shock and deceleration. At the same time the total pressure decreases rapidly indicating that the flow is being diverted from the centerline. Over the range of pressure ratios shown in figure 10, it appears that division has taken place in less than one primary nozzle diameter.

The total pressure in the region of the primary plates appears to show rather small total pressure loss (on the order of 10 percent) until the jet reaches the end of the gutter plates. It then decays almost linearly to about half its value at an $x/D_t = 4.0$. After the centerline total pressure has reached its lowest value at the flow division point, the total pressure begins to increase. This is a result of mixing with the adjacent inner jets. The centerline total pressure then exceeds the outer primary plate jet total pressure.

The increase of the centerline static pressures at the end of the gutter plates is due to the inflow of secondary air into this region.

Axial Mach Number Distribution

The centerline and primary plate region Mach numbers are shown as a function of axial distance for configuration 1 - V(1.33) over a range of pressure ratios of 2.47 to 3.52 in figure 11. These data were computed using the jet surveys given in appendix B and the primary plate static pressures. The Mach numbers were obtained using the same procedure used to obtain the pitot tube total pressure correction.

The centerline Mach number shows a supersonic expansion to an $x/D_t = 0.58$, 0.50, and 0.42 for nozzle pressure ratios of 3.52, 3.04, and 2.47, respectively (figs. 11(a), (b), and (c)). The centerline flow then decelerates to approximately Mach 0.4. It then begins mixing with the adjacent flow and gradually accelerates to as high as $M = 0.92$.

The flow along the primary plate experiences a supersonic expansion for pressure ratios of 3.52 and 3.04 until it reaches a point just upstream of the end of the gutter plates. At this point it appears to decelerate to a Mach number which approximates that which the jet would have expanded to in freely expanding from a convergent nozzle.

The jet then continues to decelerate and for a nozzle pressure ratio of 3.52 passes through the sonic point at $x/D_t = 3.1$.

The pressure ratio of 2.47 (fig. 11(c)) yields similar results but appears to show separation of the flow somewhat closer to the primary nozzle than the higher nozzle pressure data.

The ratio of the primary nozzle base pressure to the nozzle total pressure when used to calculate a free-expansion isentropic Mach number yields values that are nearly constant. This Mach number value over the range of nozzle pressure ratios of 2.47 to 3.52 is $M = 1.82$.

Pitot-Tube Profiles for Test Configurations

Figure 12 presents composite pitot-tube total pressure profiles of the jet at an axial distance of x/D = 4.0. The composite profiles are presented for each of the configurations tested. The profiles are presented at only one axial position so that a comparison of the configurations can be made. Because of the configuration structural similarity this was considered justified.

Comparison of figure 12(a), configuration 1 - V(1.33), with figure 12(b), configuration 1 - V(1.33) - E(4), shows that the addition of an ejector in this case decreases the mixing and decay of the outer jets. This is due to the ejector preventing inflow of ambient air into the outer jets. Since the survey was taken at the end of the ejector this type of profile should be expected.

Comparison of figure 12(a) with figure 12(c) shows the effect of the shorter gutter plates. The shorter gutter plates configuration 2 - V(0.75), yield a profile that has a considerably lower centerline pitot-tube pressure than the longer gutter plates of configuration 1 - V(1.33). The peaks and valleys in the profiles for configuration 2 - V(0.75) are quite pronounced when compared with configuration 1 - V(1.33). Within the region of ±3 centimeters off the axial centerline the shorter gutter plates (configuration 2 - V(0.75)) appear to cause less mixing than the longer gutter plates of configuration 1 - V(1.33).

Increasing nominal nozzle pressure ratios from 2.5 through 4.0 results in greater differences between the valleys and peaks of configuration 2 - V(0.75) than for configuration 1 - V(1.33) in the ±3 centimeters region (figs. 12(c) and (a), respectively).

For configuration 2 - V(0.75) at a pressure ratio of 2.46, it appears that an optimun pressure ratio had been reached and that further increase in nozzle pressure ratio results in an accelerated rate of jet pitot pressure increase with nozzle pressure ratio. This is objectionable because of an increase in the noise level, which is associated with increased velocity.

The addition of an ejector to configuration 2 - V(0.75) (fig. 12(d)) configuration 2 - V(0.75) - E(2), shows that this increases the pitot-tube pressure peaks. When comparing the long ejector (fig. 12(b)) with the short ejector figure 12(d) it appears that the short ejector of configuration 2 - V(0.75) - E(2) is better from the standpoint of velocity decay with axial distance.

Acoustic Measurements

Noise measurements made during tests of the plain converging primary nozzle and the divergent-multilobed nozzle are shown in figure 13. It was assumed that at least for comparison purposes the noise measurements are adequate for use in determining dif-

ferences in peak sound pressure levels. The presence of the reflecting walls shown in figure 7 could produce large errors in the absolute C-weighted sound pressure level.

The sound pressure level (SPL) at the maximum lobe noise position is shown in figure 13 for configuration 2 - V(0.75) - E(2). There is a significant attenuation observed with the nozzle. The decrease in noise level for the nozzle at a velocity of approximately 350 meters per second occurred when the flow suddenly attached to the primary plates. Thus dividing the flow into separate jets.

Thrust Loss and Noise Attenuation

The attenuation is defined by comparison with the conical nozzle and is the difference between the SPL of the conical nozzle and the SPL of the test nozzle. Figure 14(a) shows the attenuation at the maximum lobe noise position for configuration 1 - V(1.33) and 1 - V(1.33) - E(4) over the entire operating range of nozzle pressure ratios. The attenuation increases with increasing pressure ratio for the configuration without an ejector. The addition of the ejector creates a peak attenuation at a pressure ratio of 3 and then a decrease.

The attenuation is 12 decibels with the ejector installed operating at a nozzle pressure ratio of 3.5. Associated with this attenuation and pressure ratio is a high thrust loss (fig. 14(a)), which is 24 percent based on the ideal net thrust of a conical nozzle calculated as shown in the DATA REDUCTION section in this report. The thrust loss in general increases with increasing pressure ratio until the flow attaches to the primary plates. The thrust loss then decreases with increasing pressure ratio. It is necessary to discuss the attenuation along with the thrust loss because of the importance of thrust loss on airplane operating economy and performance.

Without the ejector, configuration 1 - V(1.33) gives an attenuation of 10 decibels and a thrust loss of 20.5 percent at a pressure ratio of 3.5.

Configuration 2 - V(0.75) at a pressure ratio of 3.5 and without an ejector gives an attenuation of 11 decibels (fig. 14(b)) and a thrust loss of 11.5 percent at a pressure ratio of 3.5. Using an ejector on this configuration increased the attenuation to 12 decibels and decreased the thrust loss to 9 percent at a nozzle pressure ratio of 3.5. The ratio of attenuation to thrust loss at this pressure was 1.33 decibels per percent of thrust loss. This was the best configuration tested. The addition of the ejector shroud in this case did not result in a sharp peak in the attenuation as a function of nozzle pressure ratio curve.

The dashed lines in figure 14 indicate a region in which the nozzle pressure has not reached the point where the flow attaches to the primary plates. When attachment occurs, a discontinuity occurs in both the sound level and the thrust. Hence, the dashed lines indicate an uncertainty in the flow attachment nozzle pressure ratio.

Secondary Air Flow

The secondary mass flow rate was measured as described earlier in this report. The results of these measurements are shown in figure 15 for configurations 1 - V(1.33) - E(4) and 2 - V(0.75) - E(2). Figure 15 presents the ratio of secondary to primary mass flow rates as a function of nozzle pressure ratio. The overall pumping ability of the two configurations is on the order of 30 to 40 percent of the primary weight flow rate over the nozzle pressure ratio range of 1.5 to 4.0. Configuration 2 - V(0.75) - E(2) pumps about 5 percent more flow than configuration 1 - V(1.33) - E(4) even though it had the shorter ejector. It should be kept in mind that in measuring the secondary flow the ejector operates at a reduced inlet total pressure because of the box bellmouths total-pressure loss.

CONCLUSIONS

Cold flow tests were made on a divergent-lobed nozzle consisting of eight primary plates attached at the throat station of a convergent nozzle and extending in the direction of the jet flow but diverging from the nozzle centerline at a 15° angle. Tests were run both with and without ejector shrouds. The smallest cylindrical ejector shroud was 2 primary nozzle diameters across by 2 diameters long. The nozzles were run with and without the ejector shroud. The ratio of nozzle total to ambient pressure was varied from 1.5 to 4.0. Attachment of the flow to the primary plates and splitting of the primary jet into eight smaller jets was accomplished through a nozzle pressure ratio range of 2.5 to 4.0. The following conclusions are drawn from these tests:

1. The flow from a convergent nozzle can be split into several smaller supersonic jets by arranging channel plates around the exit of the nozzle and diverging these plates from the axial centerline.

2. The resulting jets mix faster with the surrounding air than the single jet flowing from the plain convergent nozzle (Mach 1 at $x/D_t = 12$) and results in a lower peak velocity at a given distance (Mach 1 at $x/D_t = 3$) than those obtained with the plain convergent nozzle.

3. The maximum lobe (30° to 45° off jet centerline) sound pressure level of the multijet flow obtained as discussed in conclusion (1) is lower than that measured for the plain conical nozzle by 12 decibles at a pressure ratio of 3.5 to 4.0.

4. Thrust loss of the nozzle operating with the attenuation stated in conclusion (3) is 7 and 9 percent with the nozzle operating at a nozzle pressure ratio of 4 and 3.5, respectively.

5. The ratio of attenuation to thrust loss for configuration 2 - V(0.75) - E(2) (short

V-shaped gutter length) at a pressure ratio of 3.5 was 1.33 decibels per percent of thrust loss. This indicates a reasonable noise suppression for the thrust loss incurred for a nozzle operating around a nozzle pressure ratio of 3.5.

6. The secondary mass flow rate pumped by the resulting multipeaked jet configuration was as much as 44 percent of the primary nozzle flow.

Lewis Research Center,
National Aeronautics and Space Administration,
Cleveland, Ohio, December 6, 1971,
132-80.

APPENDIX A

SYMBOLS

A area, m^2

D_t primary nozzle throat diameter, m

F thrust, N

K orifice coefficient equal 0.672 in this work

L length, m

M Mach number

P total pressure, N/m^2

p static pressure, N/m^2

R gas constant, N-m/kg-K

T total temperature, K

t static temperature, K

V velocity, m/sec

W mass flow rate, kg/sec

x axial distance measured from the primary nozzle exit or throat station, m

Y the orifice expansion coefficient, equal to 0.995 in this report

γ ratio of specific heats

ρ density, kg/m^3

Subscripts:

b bellmouth

e ejector

j jet

N nozzle inlet

n net

o atmosphere

or orifice

p primary

s secondary

t throat

v V-shaped gutter plate

1 orifice upstream

2 orifice downstream

APPENDIX B

PITOT TOTAL AND STATIC PRESSURE PROFILES AT VARYING AXIAL DISTANCES

The data used to determine the Mach number of the flow along the primary plates and the nozzle centerline were recorded using an x-y-y' plotter. The pitot-tube total- and static-pressure profiles used to calculate the Mach numbers for configuration 1 - V(1.33) are given here. A sufficient number of the profiles are given so that a detailed picture of the flow field through configuration 1 - V(1.33) can be obtained if desired. The profiles are given through an axial distance range of x/D_t of 0 to 4. The data are presented in figures 16 to 18.

REFERENCES

1. Lighthill, M. J.: Jet Noise. AIAA J., vol. 1, no. 7, July 1963, p. 1507-1517.

2. Greatrex, F. B.: Jet Noise. Proceedings of the Fifth International Aeronautical Conference, June 1955, pp. 415-448.

3. Eldred, Kenneth M.; White, Robert W.; Mann, Myron A.; and Cottis, Miltiades G.: Suppression of Jet Noise With Emphasis on the Near Field. Western Electro-Acoustic Lab., Inc. (ASD-TDR-62-578), Feb. 1963, pp. 101-102.

4. Anon.: ASME Power Test Codes, Supplement on Instruments and Apparatus, Part 5 - Measurement of Quantity of Materials PTC 19.5, 4-1959.

5. Nagamatsu, H. T.; Sheer, R. E., Jr.; and Horvay, G.: Supersonic Jet Noise Theory and Experiments. Basic Aerodynamic Noise Research. NASA SP-207, 1969, pp. 17-51.

6. Ames Research Staff: Equations, Tables, and Charts for Compressible Flow. NACA Rep. 1135, 1953.

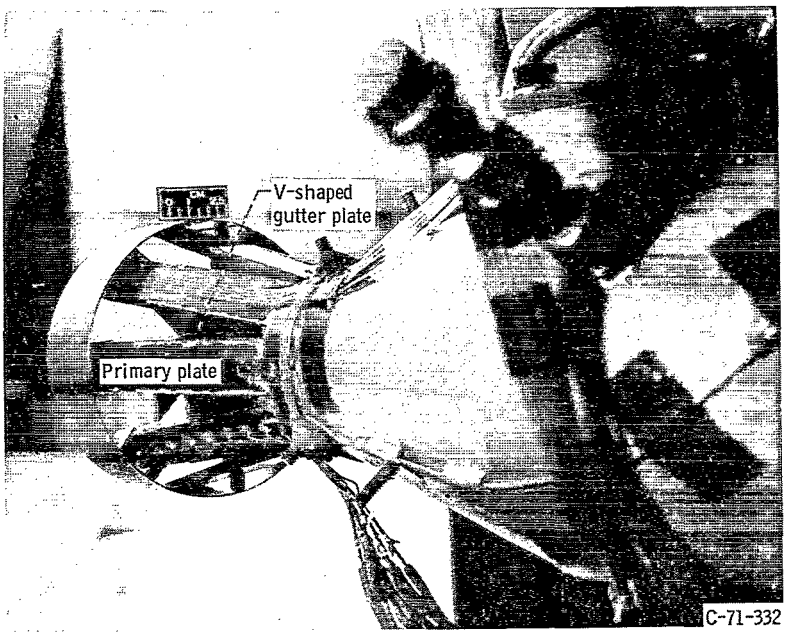

(a) Nozzle viewed in direction of jet efflux.

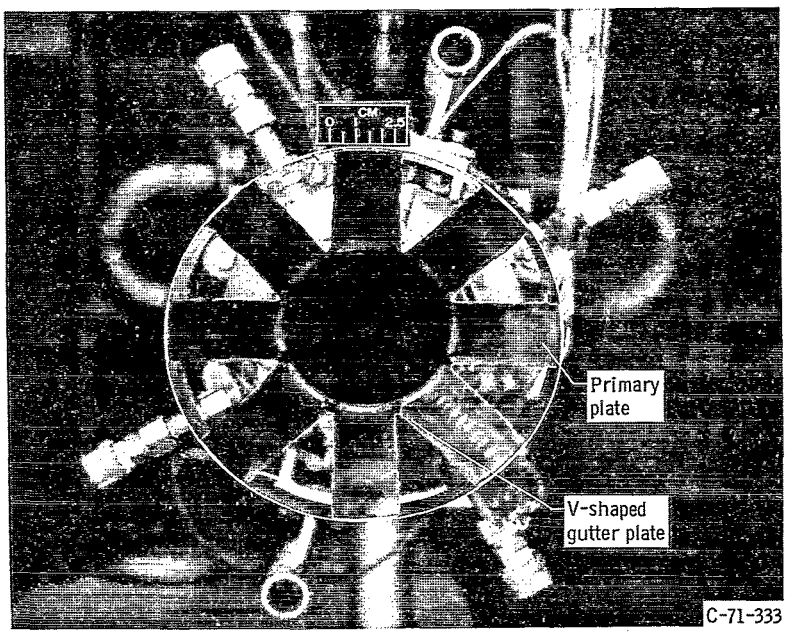

(b) Rear view of nozzle.

Figure 1. - Divergent lobed nozzle as installed in test facility; configuration 1-V(1.33).

Configuration	L_p, cm	L_V, cm	L_E, cm
1-V(1.33)	13.49	10.16	-----
1-V(1.33)-E(4)	13.49	10.16	30.48
2-V(0.75)	10.59	5.72	-----
2-V(0.75)-E(2)	10.59	5.72	15.24

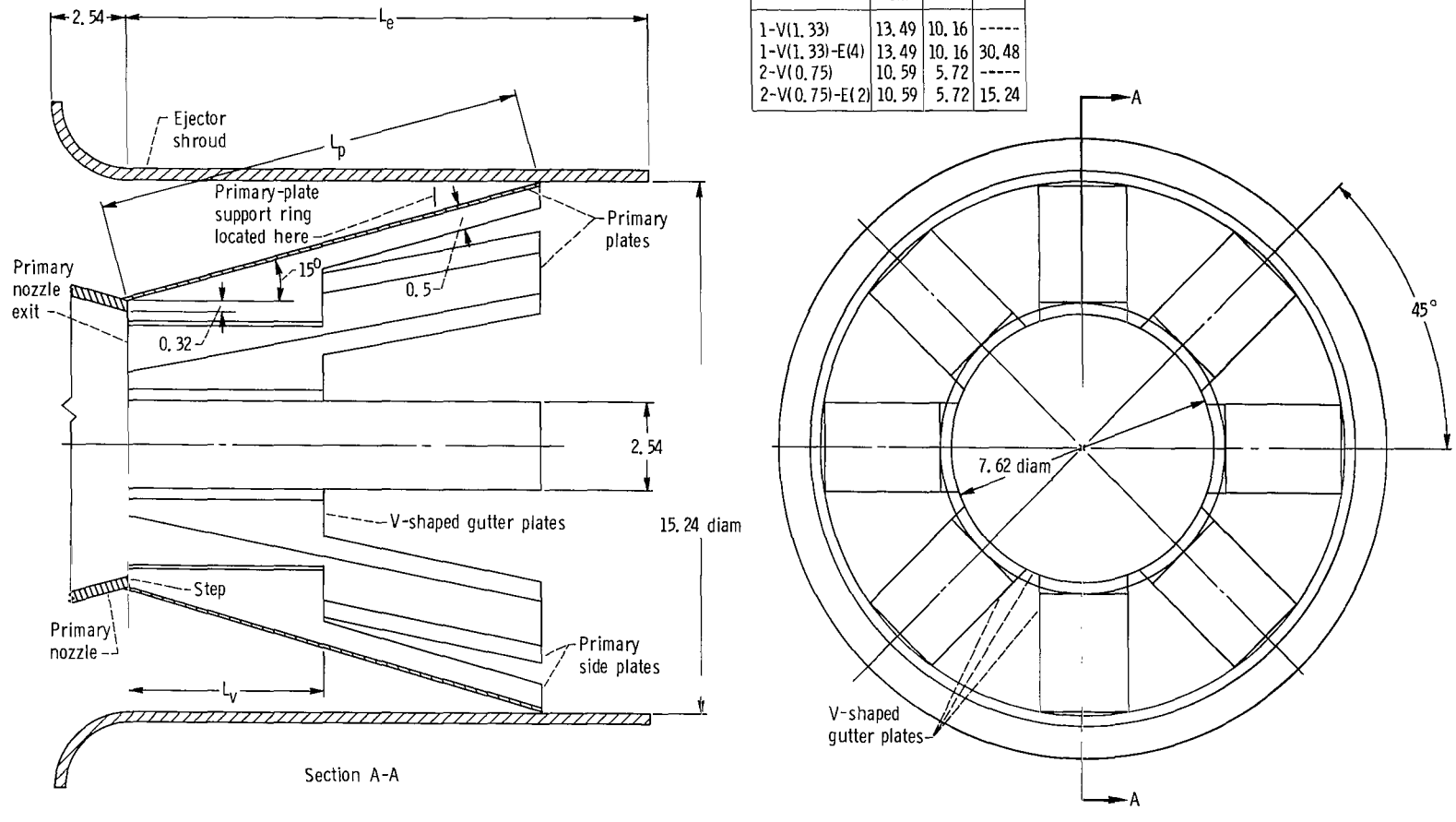

Figure 2. - Divergent lobed nozzle. (All linear dimensions are in centimeters.)

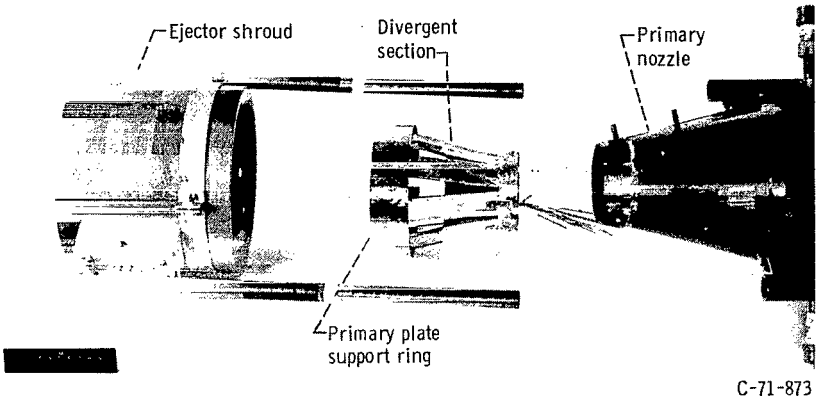

Figure 3. - Exploded view of ejector shroud, divergent section of nozzle, and primary nozzle.

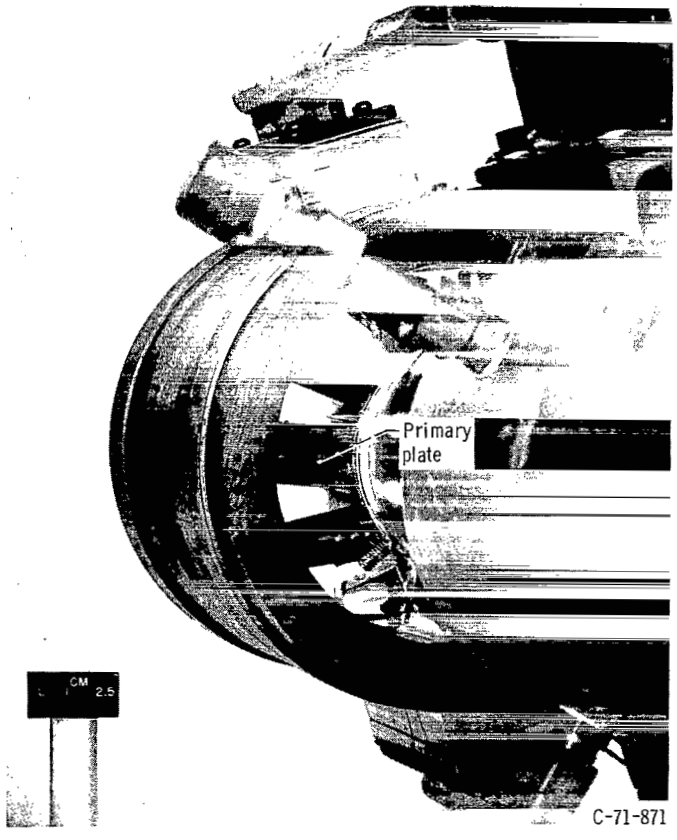

(a) Nozzle viewed in direction of jet efflux.

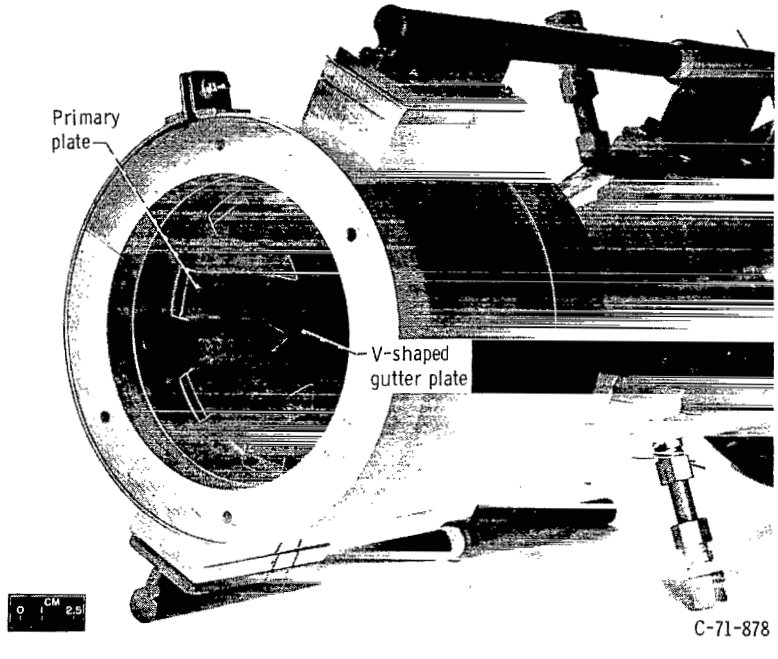

(b) Rear oblique view of divergent section V-shaped gutter plates and truncated primary plates.

Figure 4. - Divergent lobed nozzle with ejector installed; configuration 2 - V(0.75) - E(2).

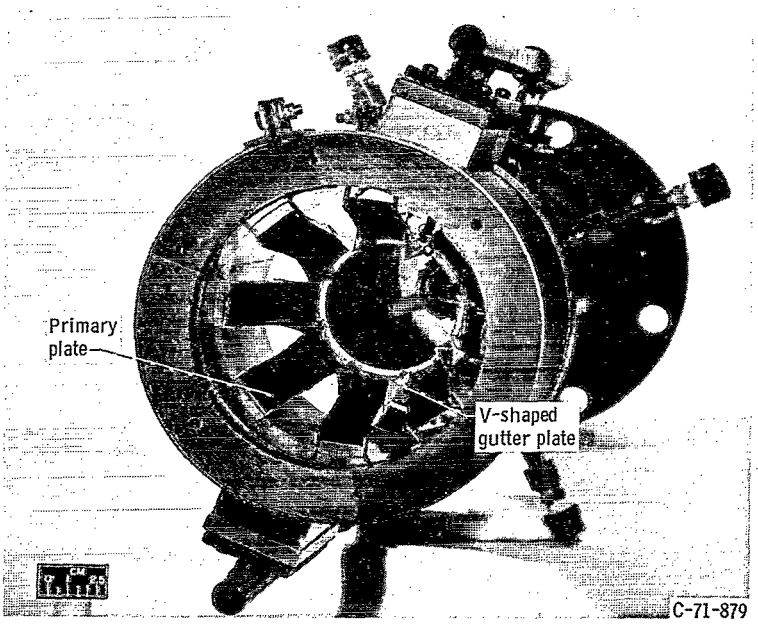

(c) Rear oblique view of primary nozzle base step.

Figure 4. - Concluded.

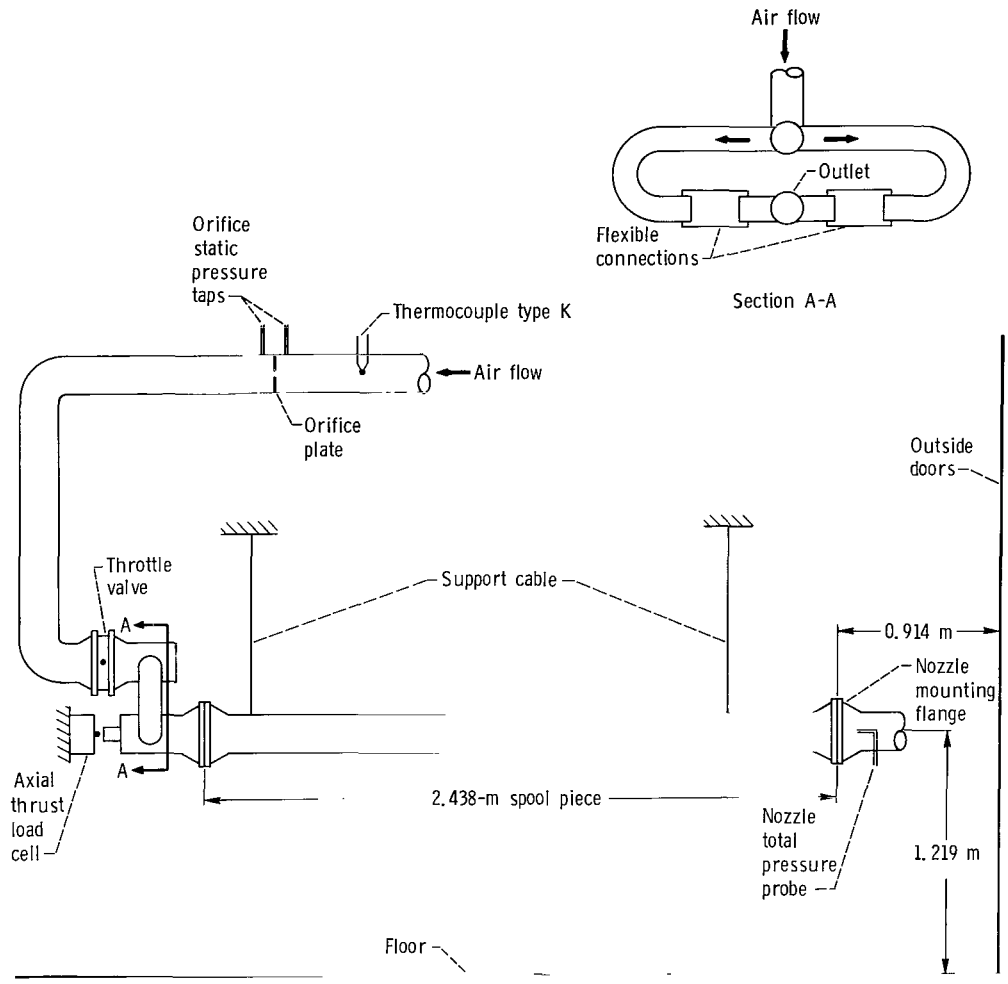

Figure 5. - Air flow and thrust measuring system.

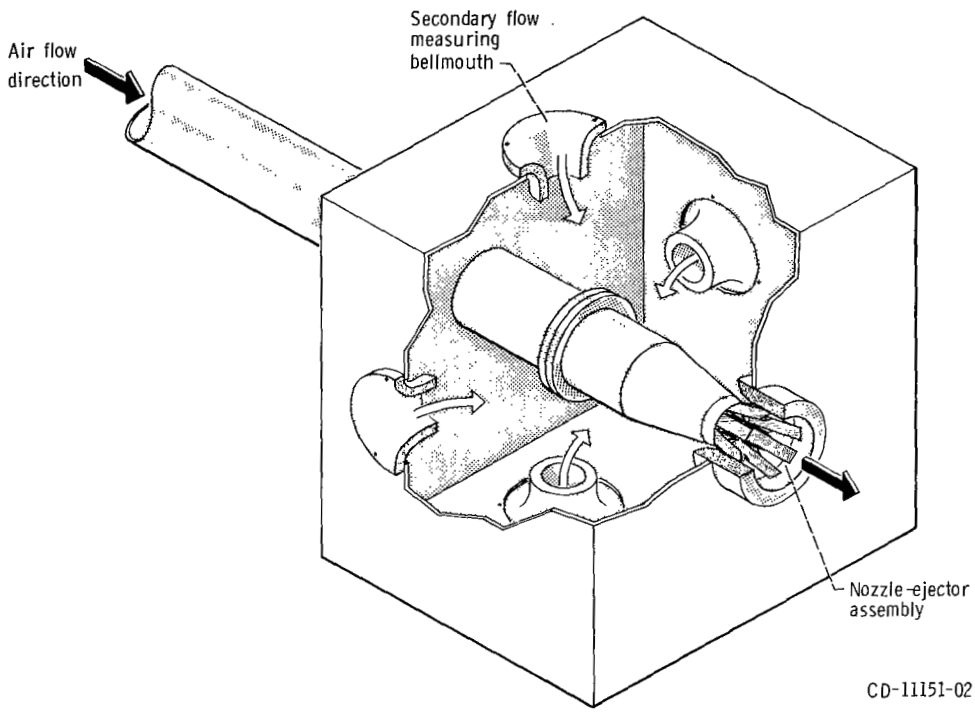

Figure 6. - Secondary box enclosing ejector inlet with secondary flow measuring bellmouths.

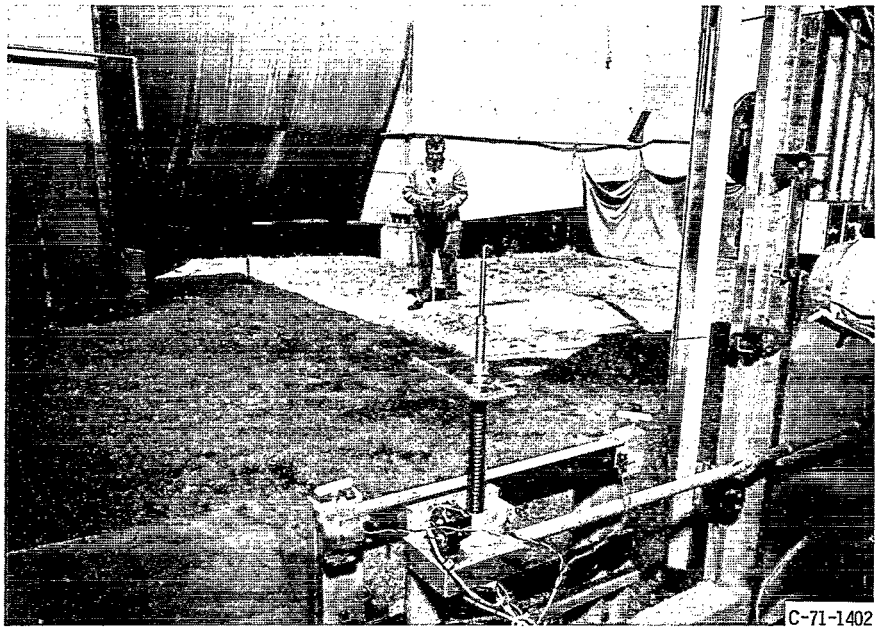

(a) Sound measurements being taken at 30° angular location of jet centerline using hand held meter.

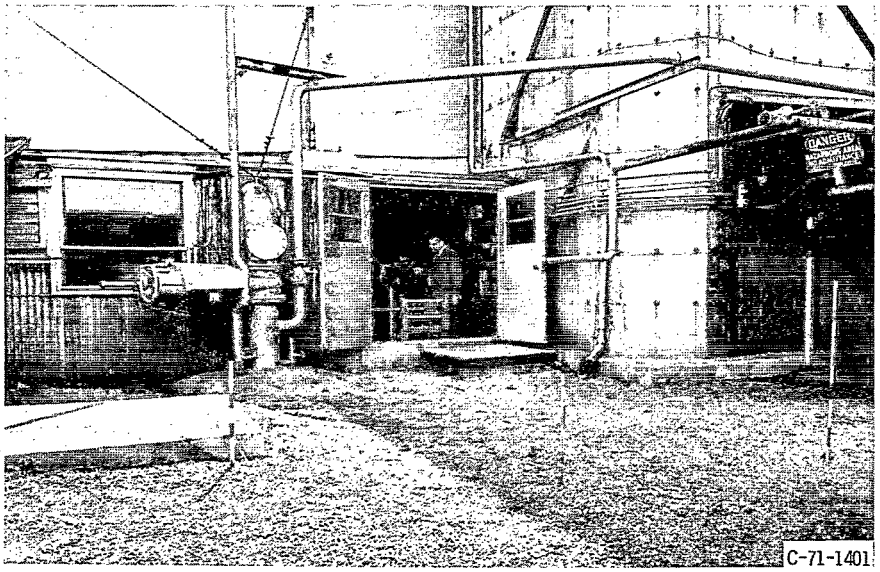

(b) View of court yard looking toward nozzle from the 20° location of centerline.

Figure 7. - Court yard used for jet noise measurements.

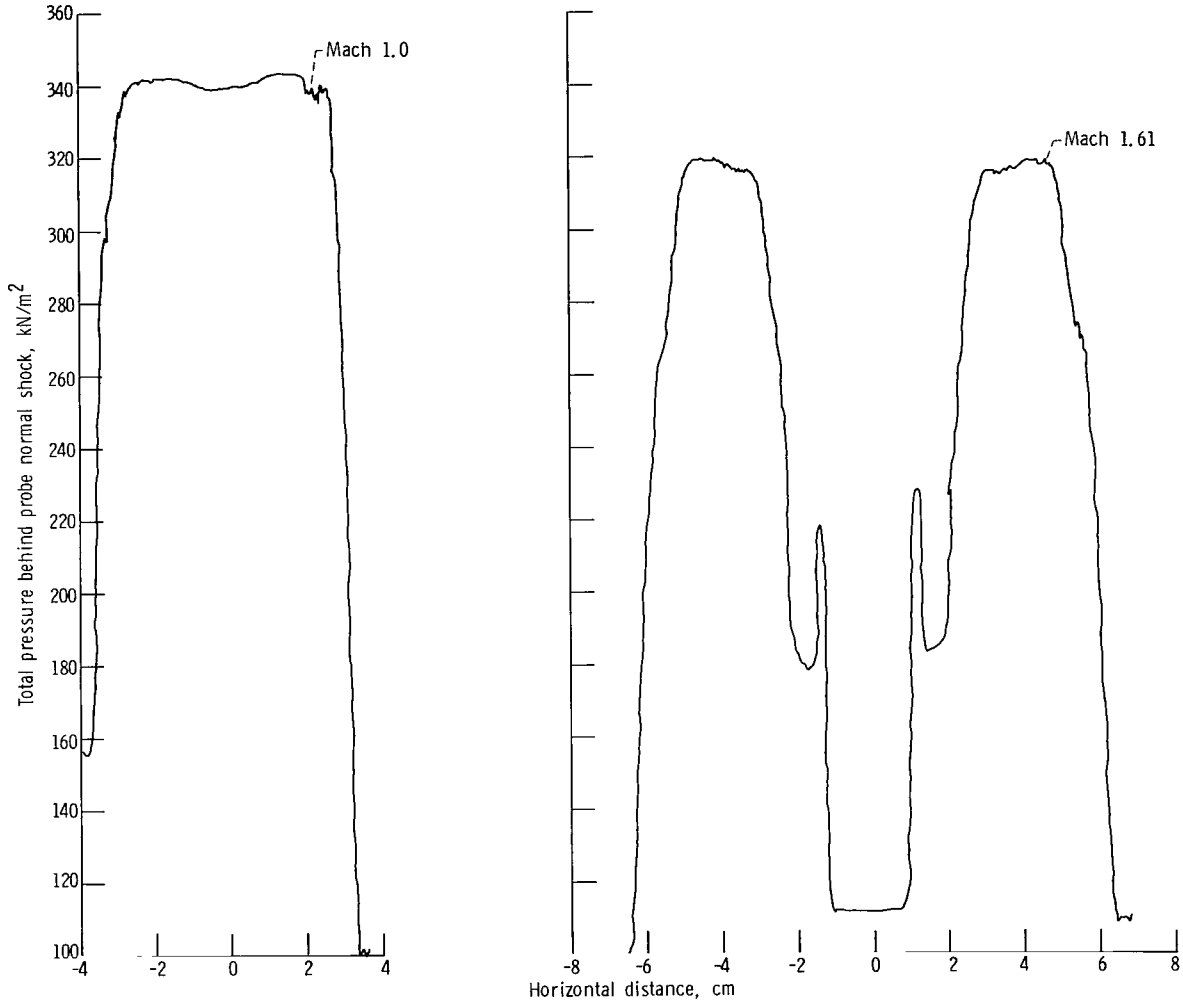

(a) Throat station (x/D_t = 0).

(b) End of V-shaped gutter plates (x/D_t = 1.33).

Figure 8. - Pitot-tube total pressure profile normal to jet axis centerline; configuration 1 - V(1.33); nozzle pressure ratio, 3.52.

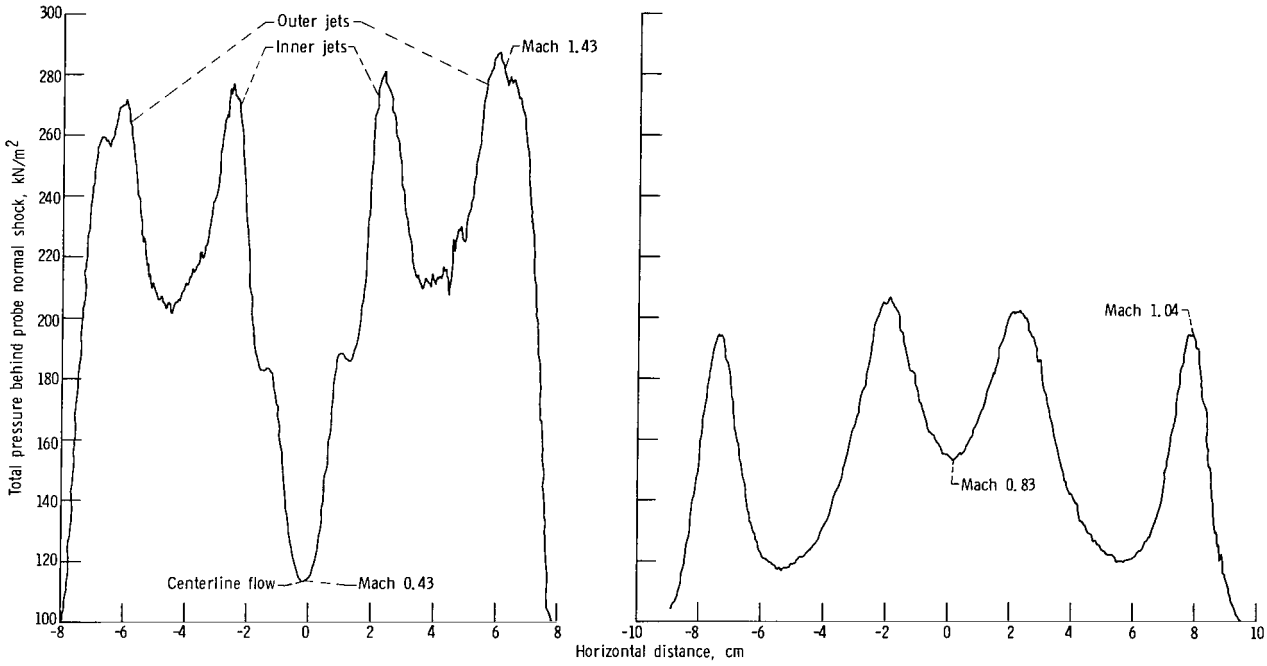

(c) End of primary plate (x/D_t = 1.85).

(d) Outer jet at sonic velocity (x/D_t = 3.00).

Figure 8. - Continued.

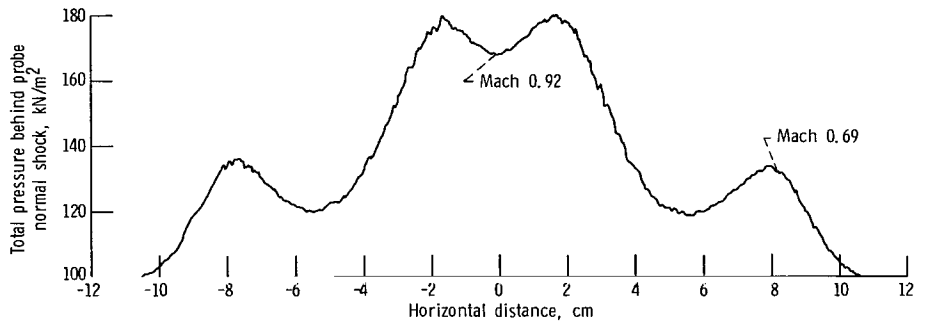

(e) Subsonic flow, centerline flow energized (x/D_t = 4.00).

Figure 8. - Concluded.

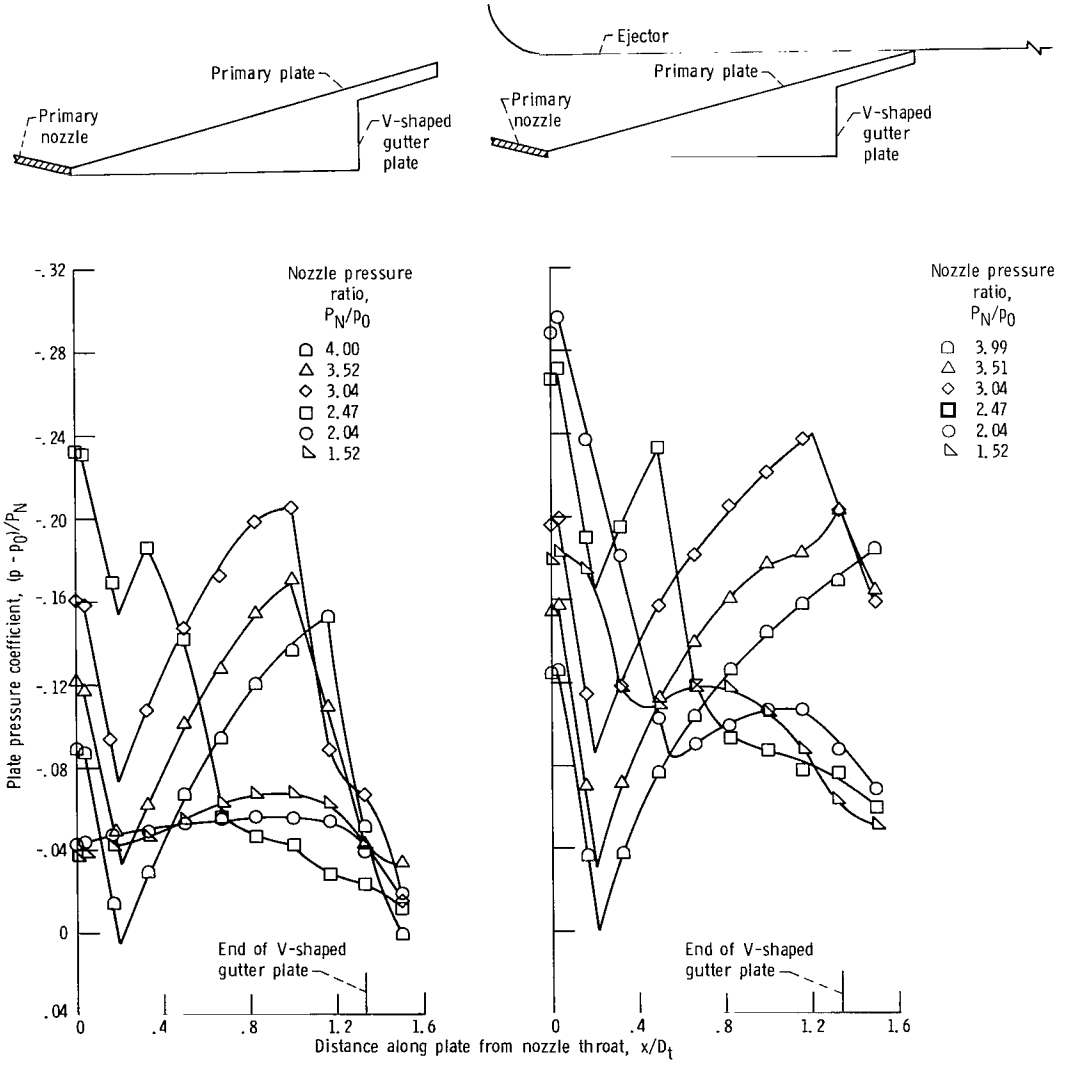

(a) Configuration 1 - V(1.33).

(b) Configuration 1 - V(1.33) - E(4).

Figure 9. - Static pressure distribution along plate surface.

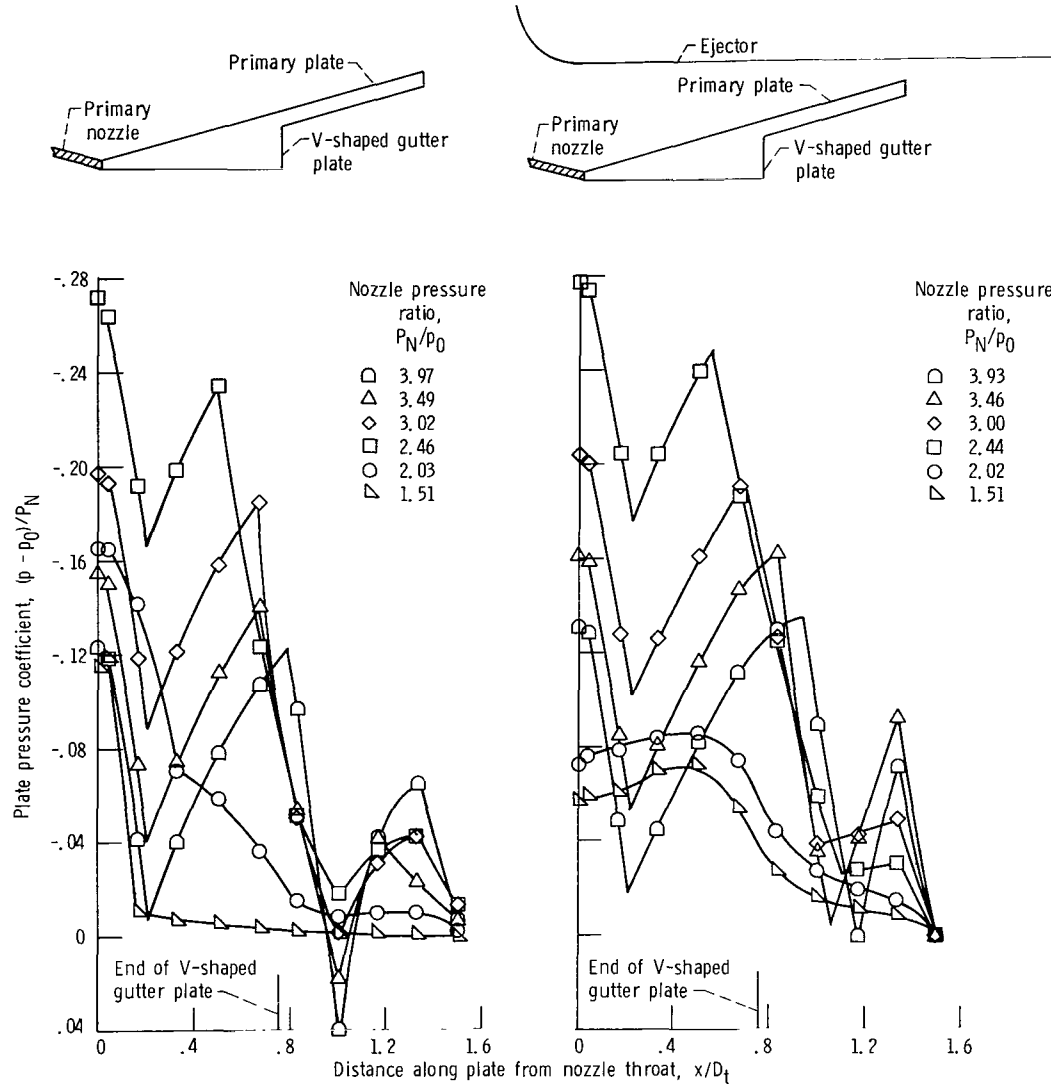

(c) Configuration 2 - V(0.75).

(d) Configuration 2 - V(0.75) - E(2).

Figure 9. - Concluded.

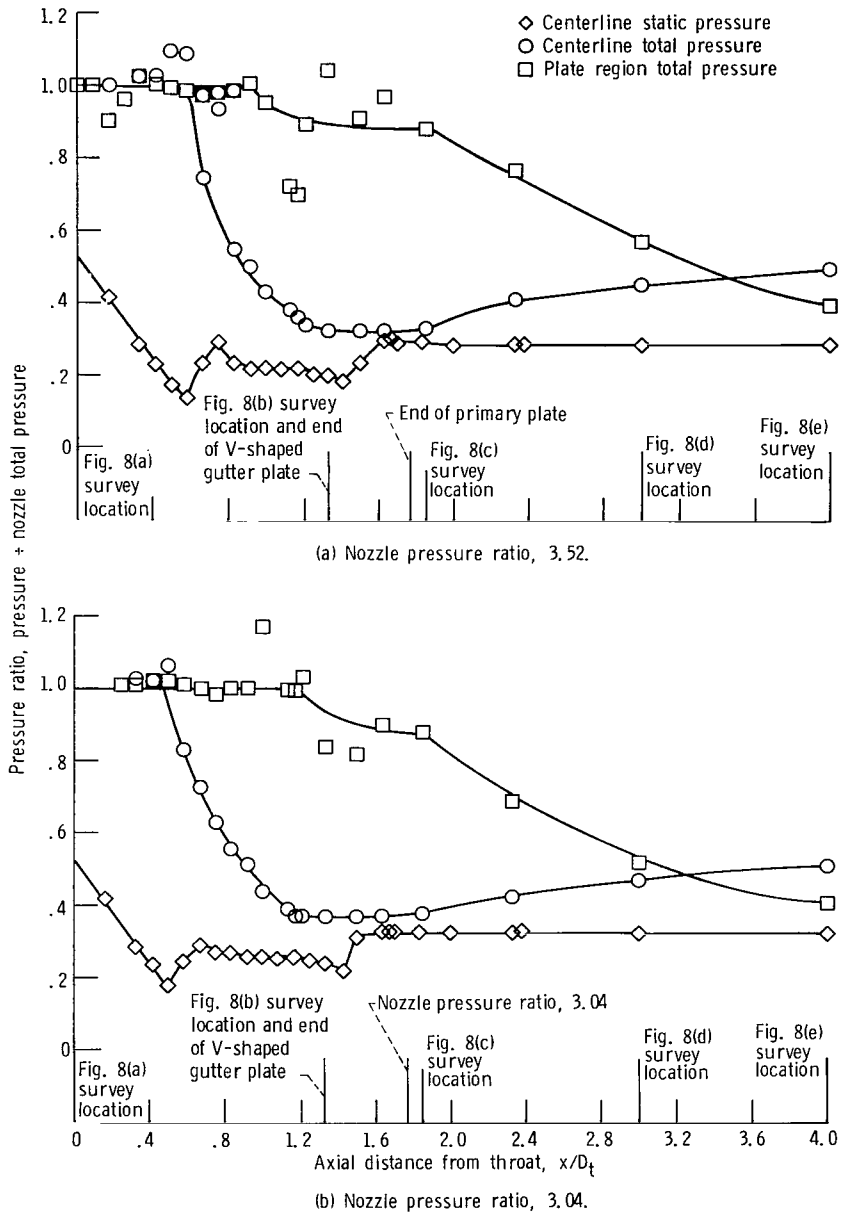

(a) Nozzle pressure ratio, 3.52.

(b) Nozzle pressure ratio, 3.04.

Figure 10. - Variation of centerline total and static pressure and plate region total pressure with axial distance from nozzle throat station. Configuration 1 - V(1.33).

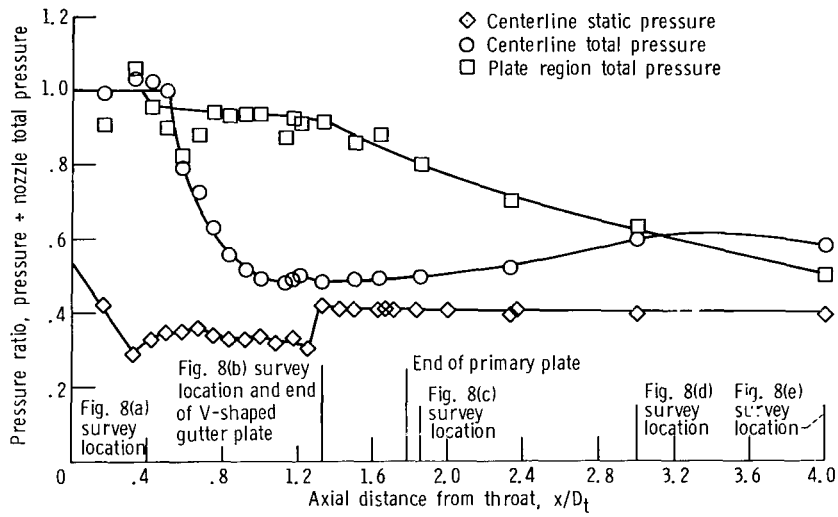

(c) Nozzle pressure ratio, 2.47.

Figure 10. - Concluded.

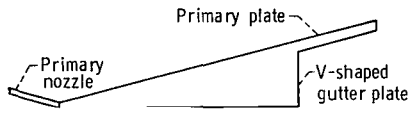

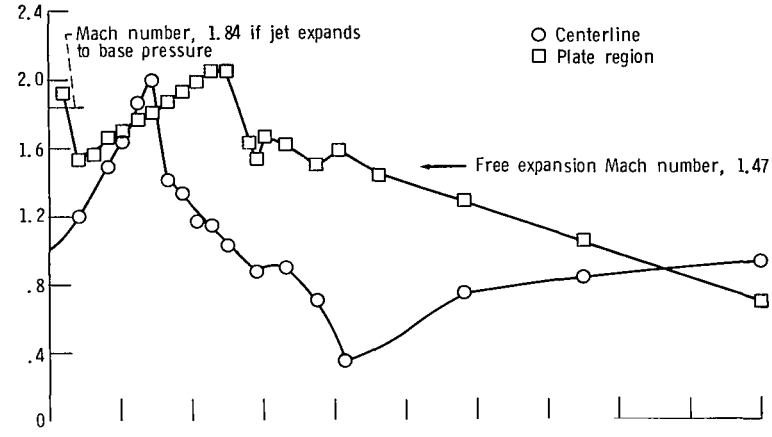

(a) Nozzle pressure ratio, 3.52.

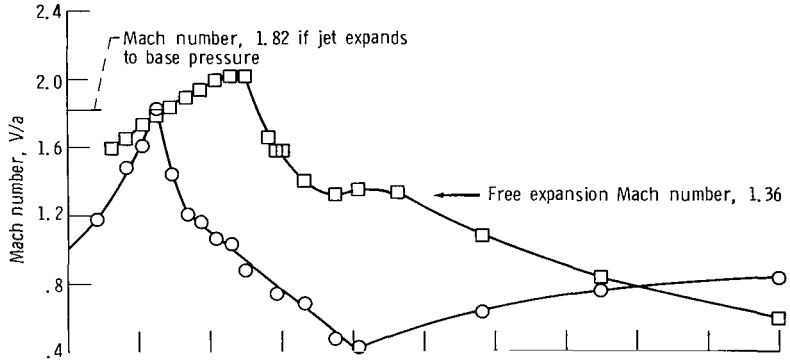

(b) Nozzle pressure ratio, 3.04.

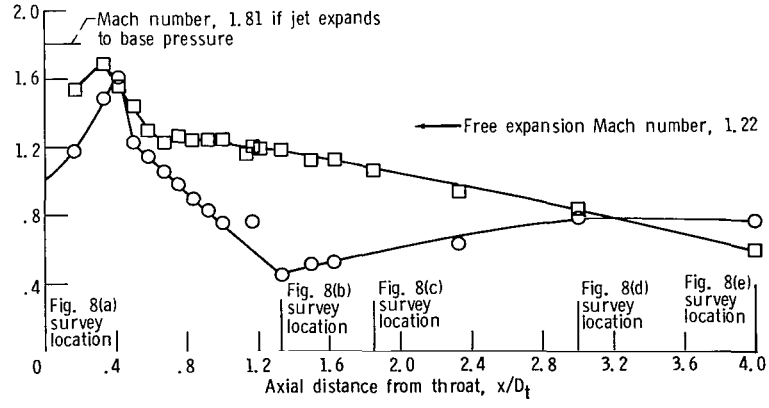

(c) Nozzle pressure ratio, 2.47.

Figure 11. - Mach number distribution along primary plate and nozzle centerline as function of axial distance from nozzle throat station. Configuration 1 - V(1.33).

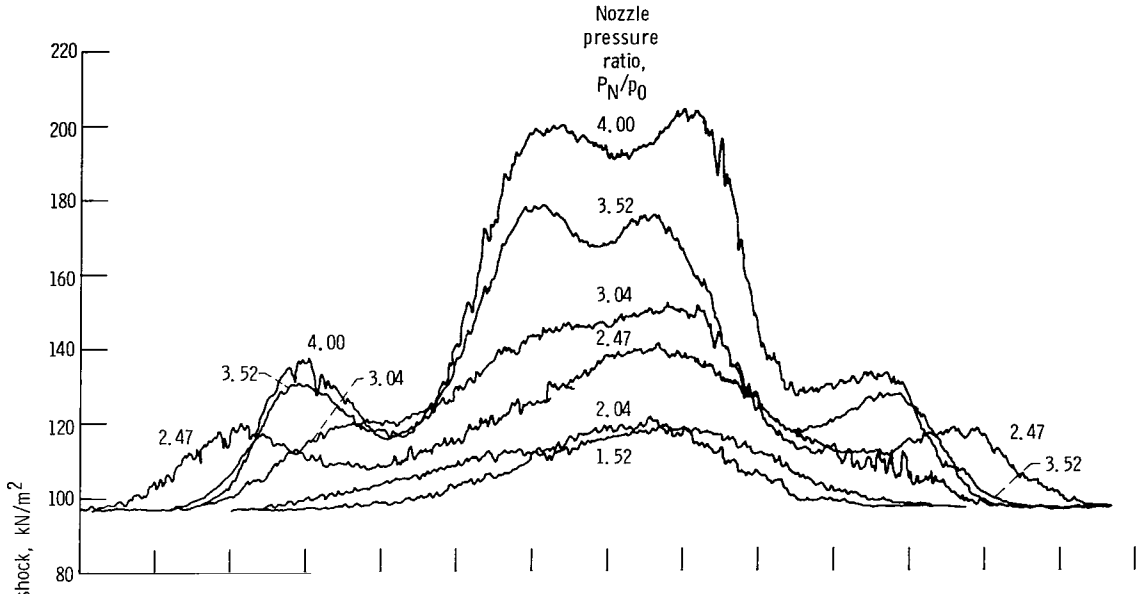

(a) Configuration 1 - V(1.33).

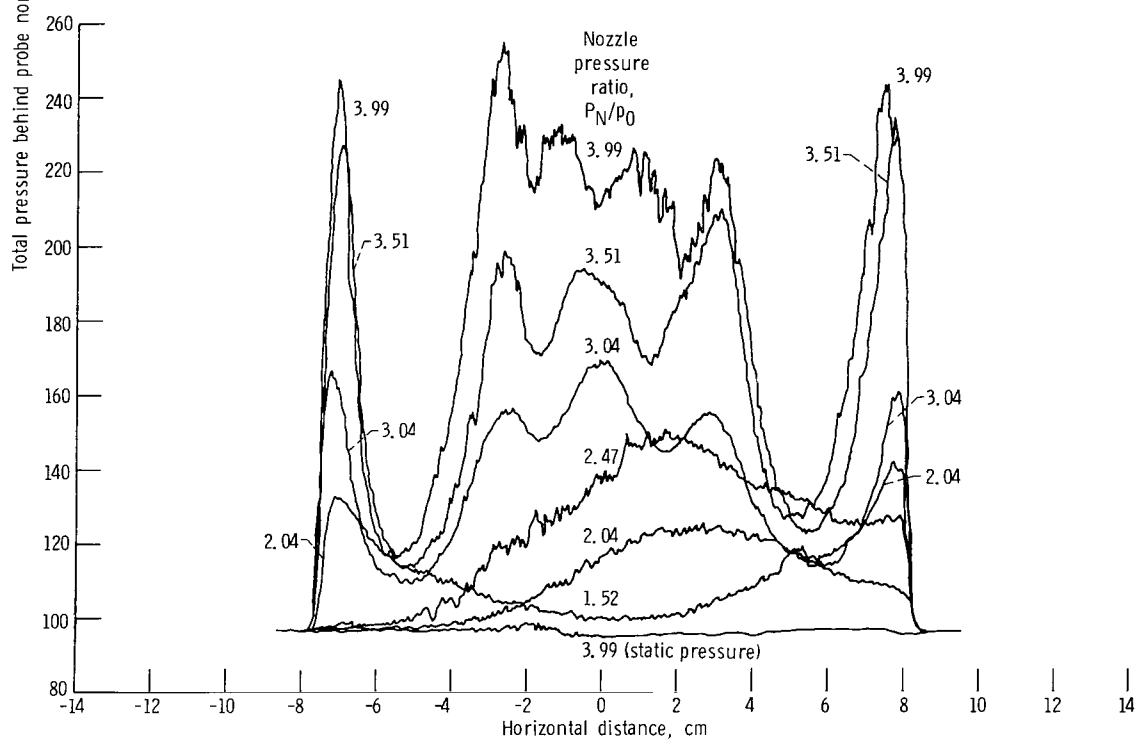

(b) Configuration 1 - V(1.33) - E(4).

Figure 12. - Pitot-tube total pressure profile across horizontal centerline of jet at $x/D_t = 4.0$.

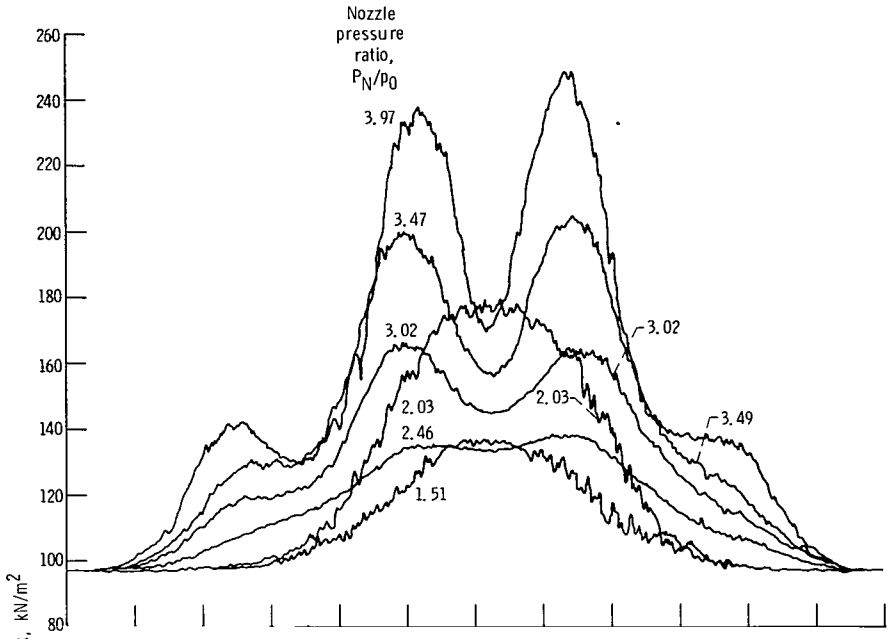

(c) Configuration 2 - V(0.75).

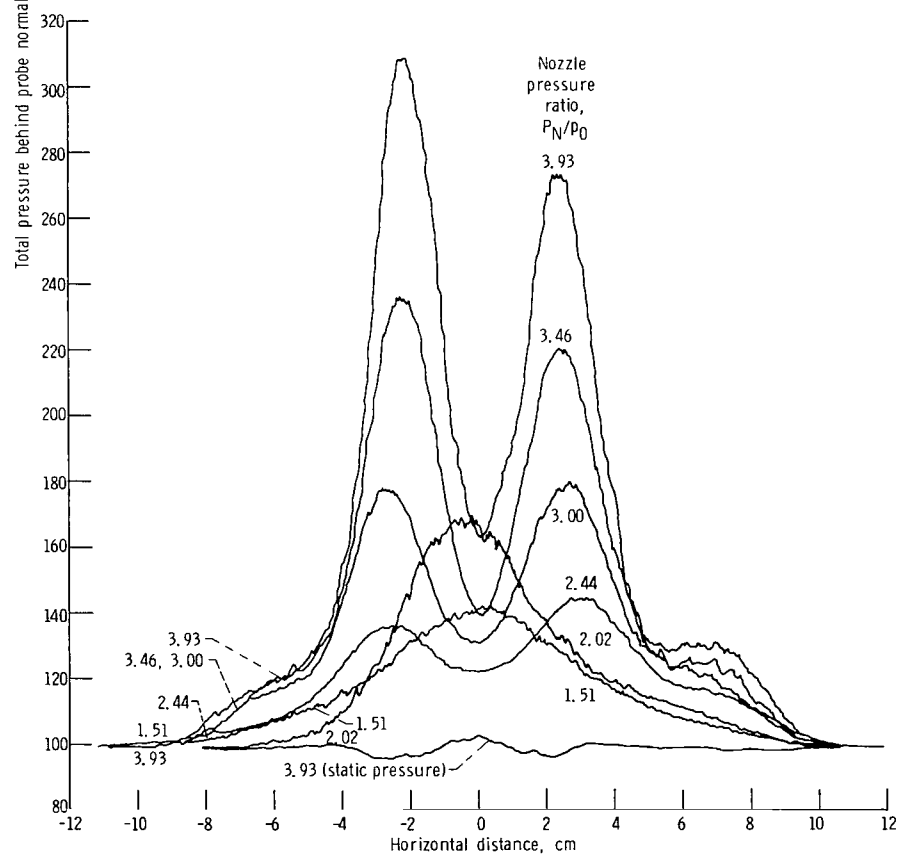

(d) Configuration 2 - V(0.75) - E(2).

Figure 12. - Concluded.

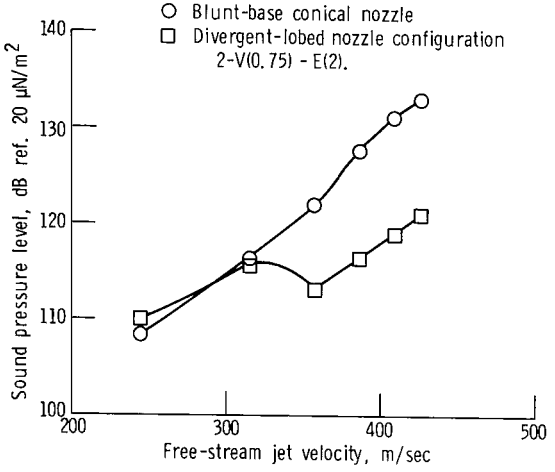

Figure 13. - C-weighted overall sound pressure level as function of isentropically expanded jet velocity, for current test conical nozzle and divergent lobed nozzle. Sound pressure level measured at 30° maximum lobe noise location using the C-weighting network.

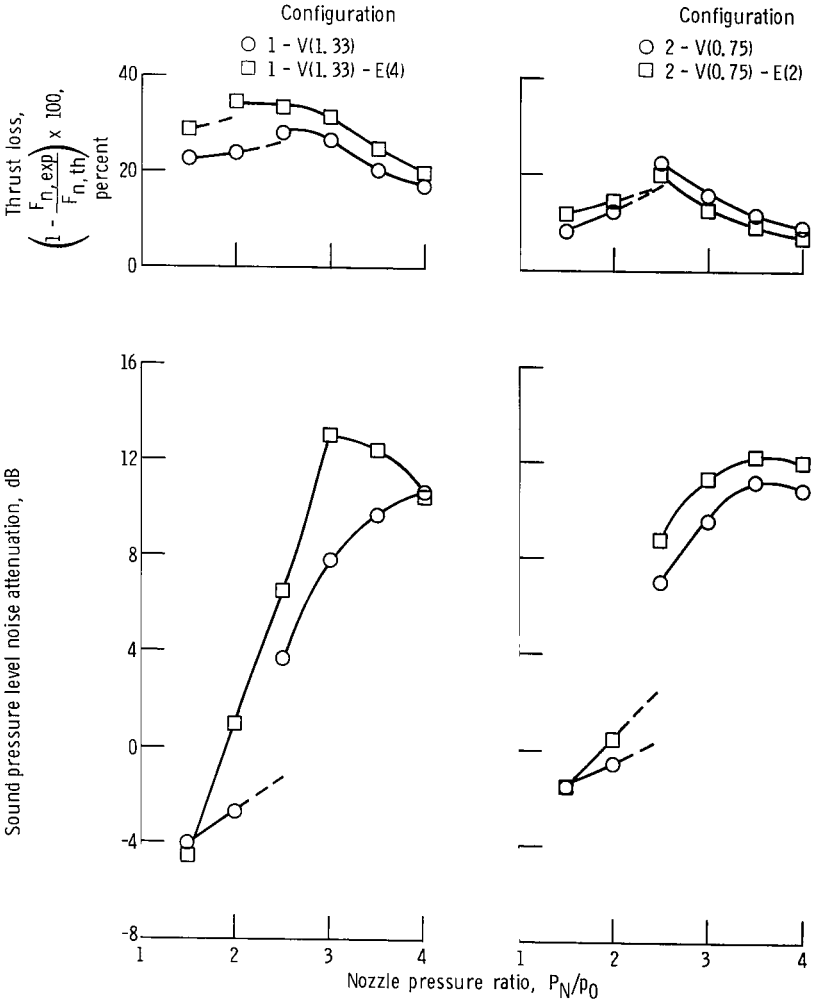

(a) Configurations 1 - V(1.33) and 1 - V(1.33) - E(4).

(b) Configurations 2 - V(0.75) and 2 - V(0.75) - E(2).

Figure 14. - Thrust loss and maximum lobe sound pressure level attenuation as functions of nozzle pressure ratio for configurations with and without ejectors.

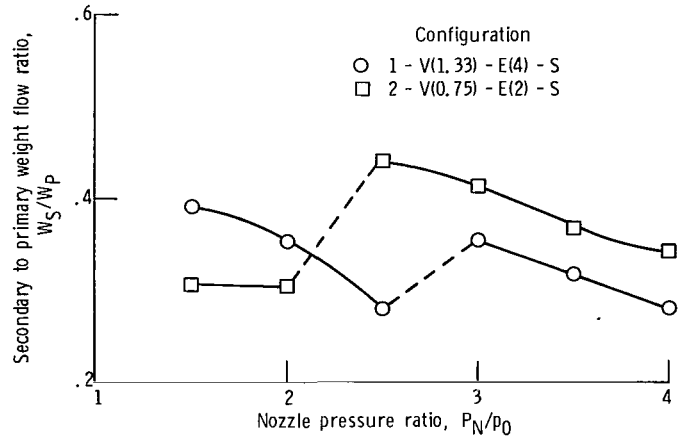

Figure 15. - Ejector weight flow as function of nozzle pressure ratio for two configurations.

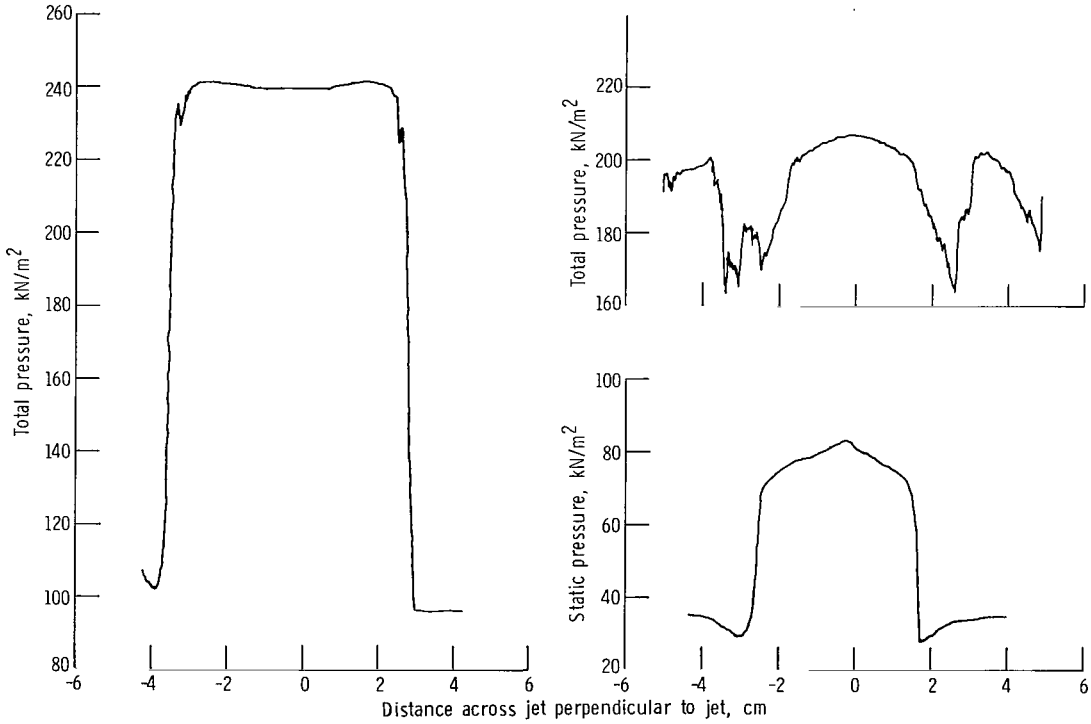

(a) Distance along plate from nozzle throat, x/D_t, 0.

(b) Distance along plate from nozzle throat, x/D_t, 0.5.

Figure 16. - Pitot total and static pressure profiles perpendicular to the nozzle centerline and through the center of opposing primary plates. Nozzle pressure ratio, 2.5.

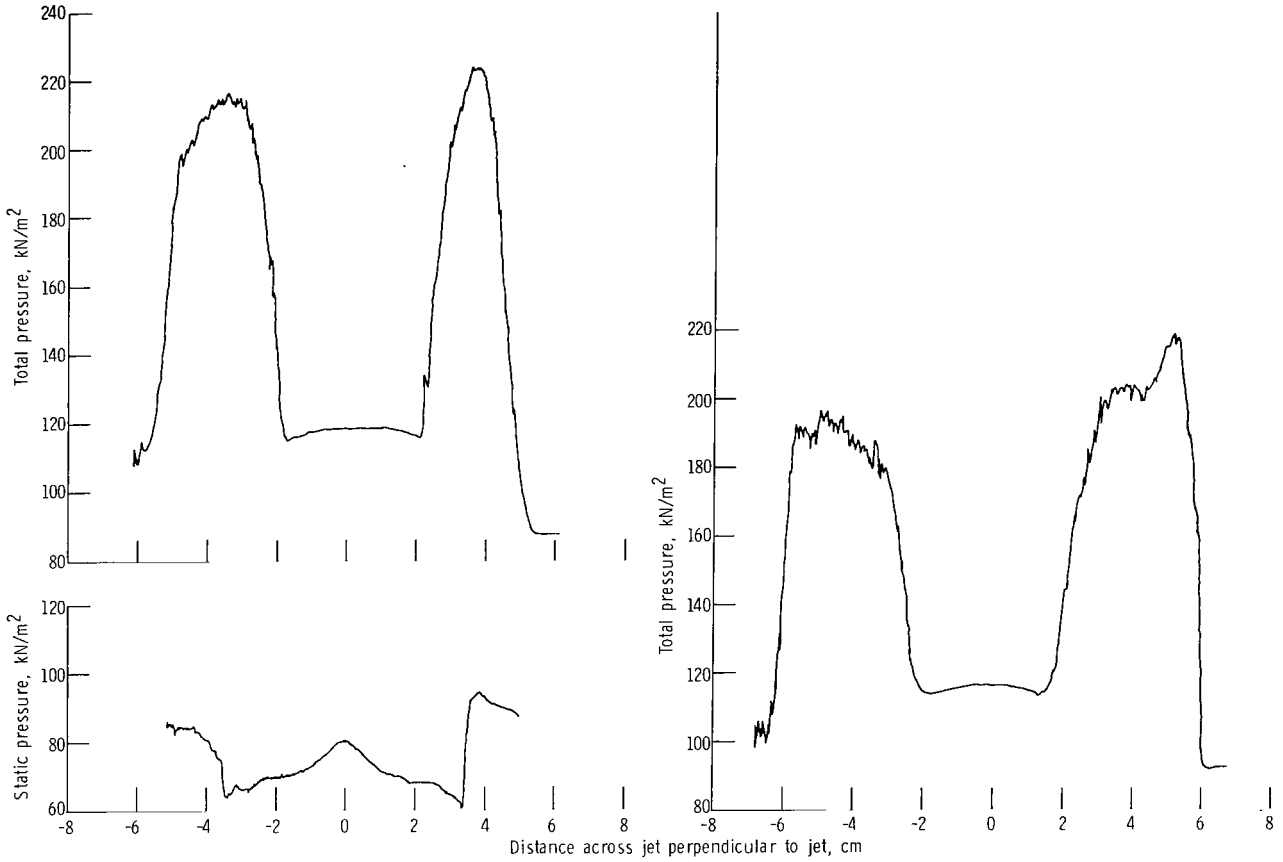

(c) Distance along plate from nozzle throat, x/D_t, 1.0.

(d) Distance along plate from nozzle throat, x/D_t, 1.33.

Figure 16. - Continued.

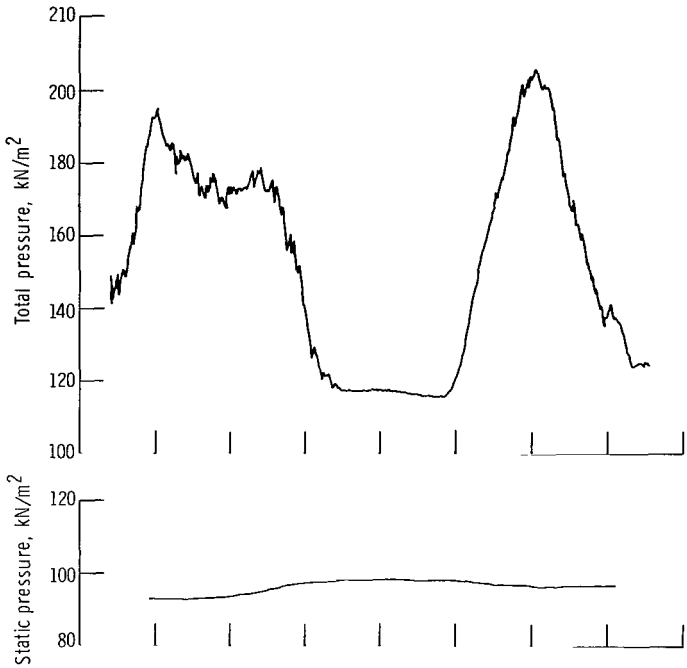

(e) Distance along plate from nozzle throat, x/D_t, 1.5.

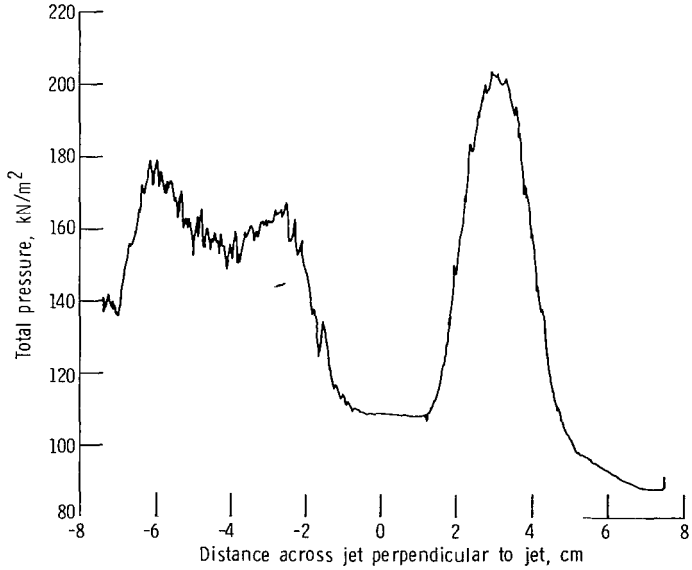

(f) Distance along plate from nozzle throat, x/D_t, 1.63.

Figure 16. - Continued.

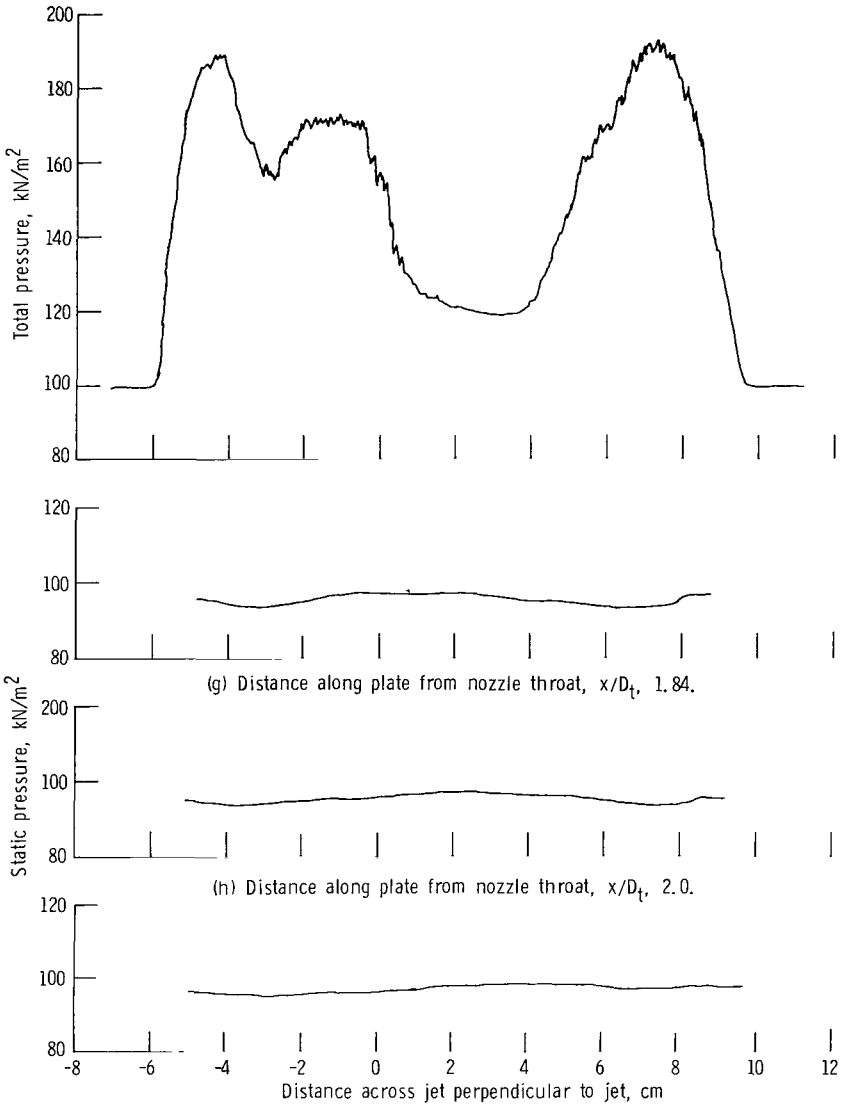

(g) Distance along plate from nozzle throat, x/D_t, 1.84.

(h) Distance along plate from nozzle throat, x/D_t, 2.0.

(i) Distance along plate from nozzle throat, x/D_t, 2.14.

Figure 16. - Continued.

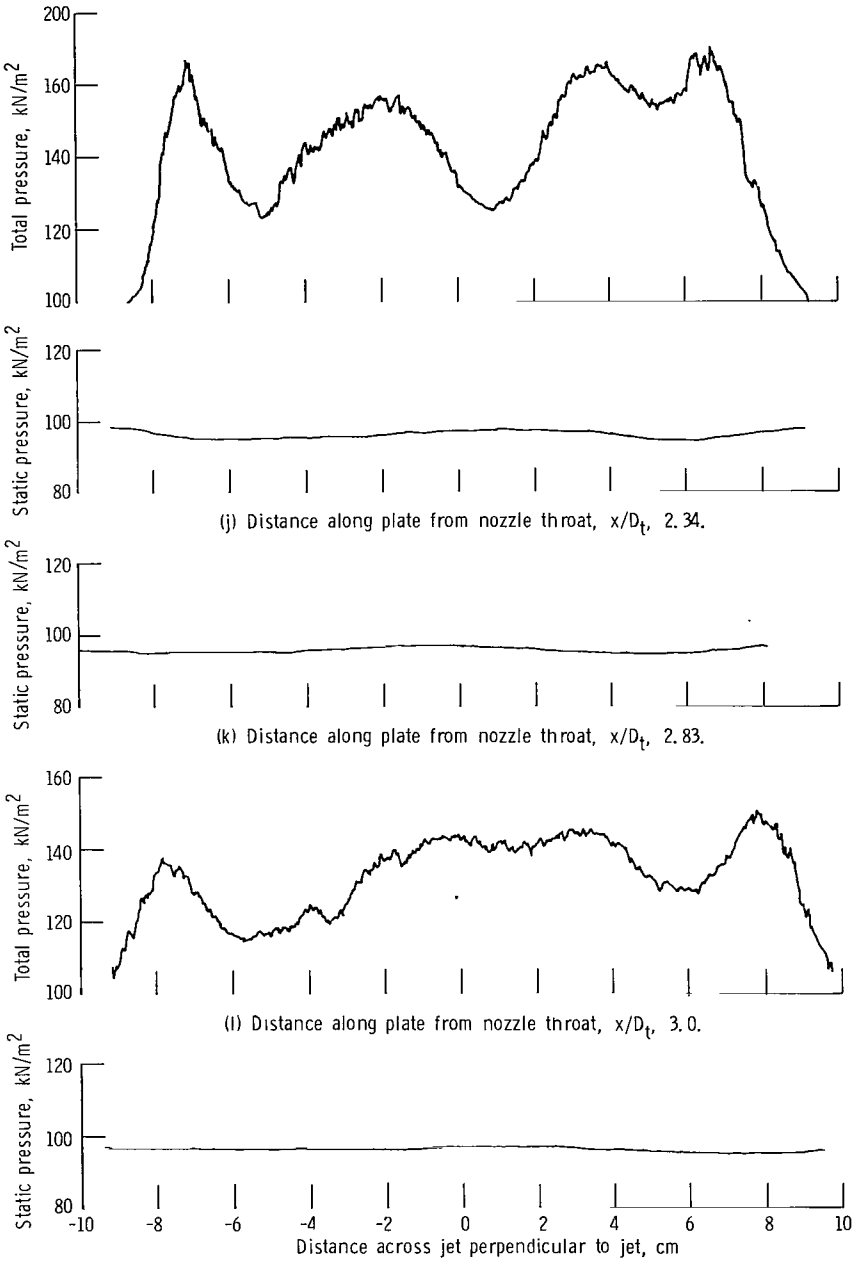

(j) Distance along plate from nozzle throat, x/D_t, 2.34.

(k) Distance along plate from nozzle throat, x/D_t, 2.83.

(l) Distance along plate from nozzle throat, x/D_t, 3.0.

(m) Distance along plate from nozzle throat, x/D_t, 3.5.

Figure 16. - Continued.

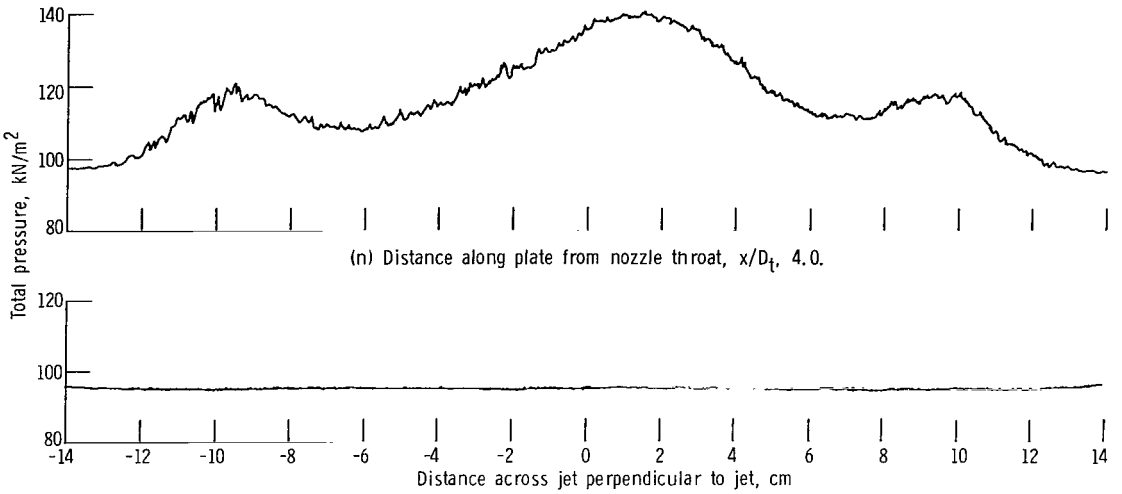

(n) Distance along plate from nozzle throat, x/D_t, 4.0.

(o) Distance along plate from nozzle throat, x/D_t, 4.5.

Figure 16. - Concluded.

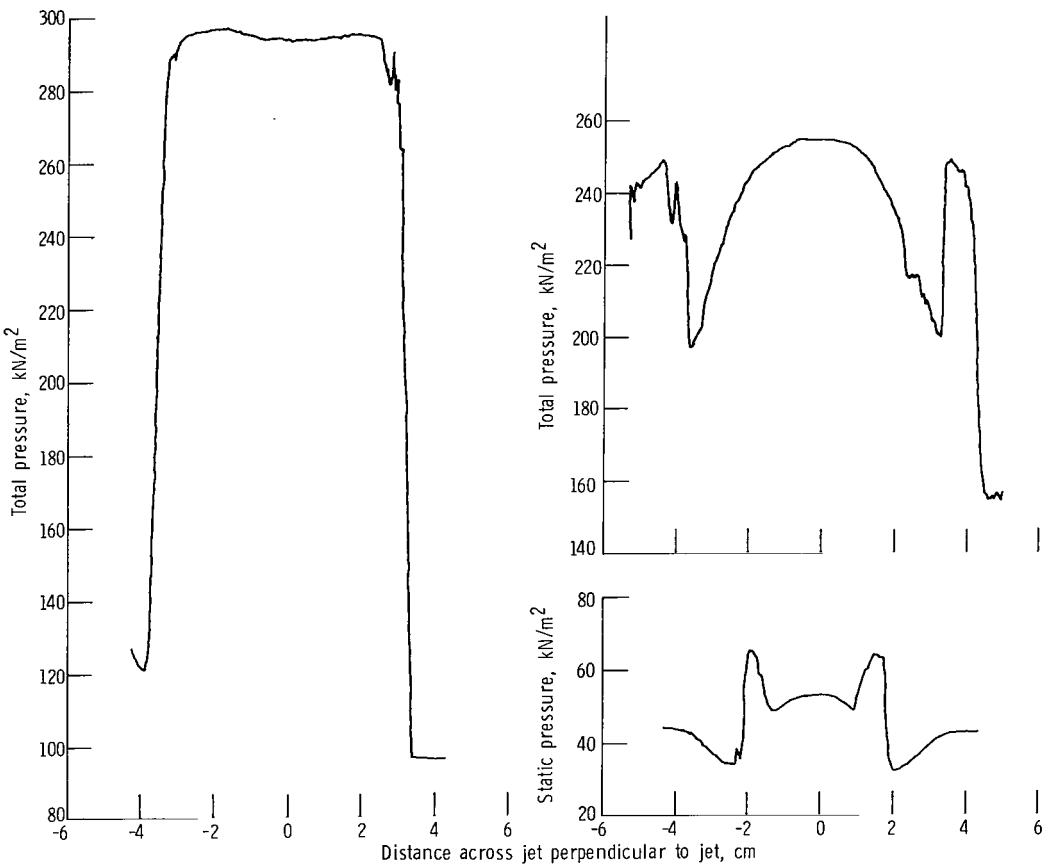

(a) Distance along plate from nozzle throat, x/D_t, 0.

(b) Distance along plate from nozzle throat, x/D_t, 0.5.

Figure 17. - Pitot and static pressure profiles perpendicular to nozzle centerline and through the center of opposing primary plates. Nozzle pressure ratio, 3.0.

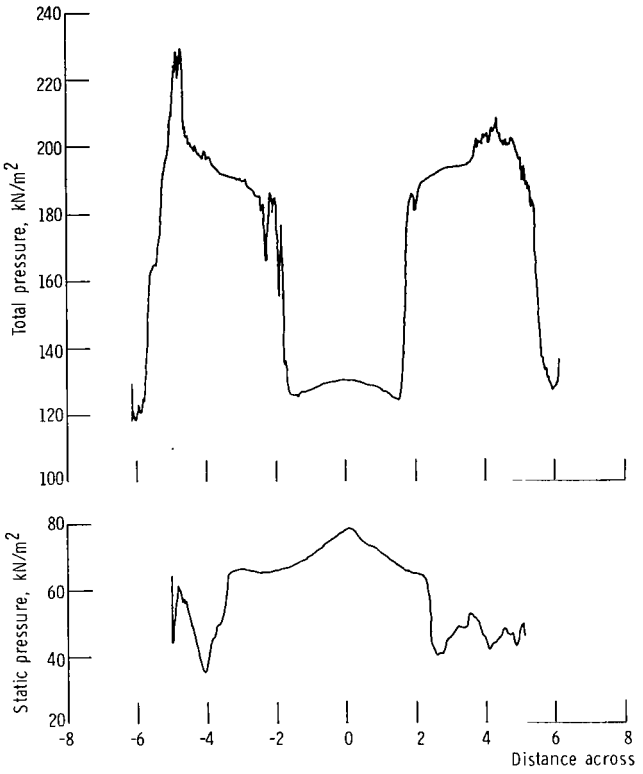

(c) Distance along plate from nozzle throat, x/D_t, 1.0.

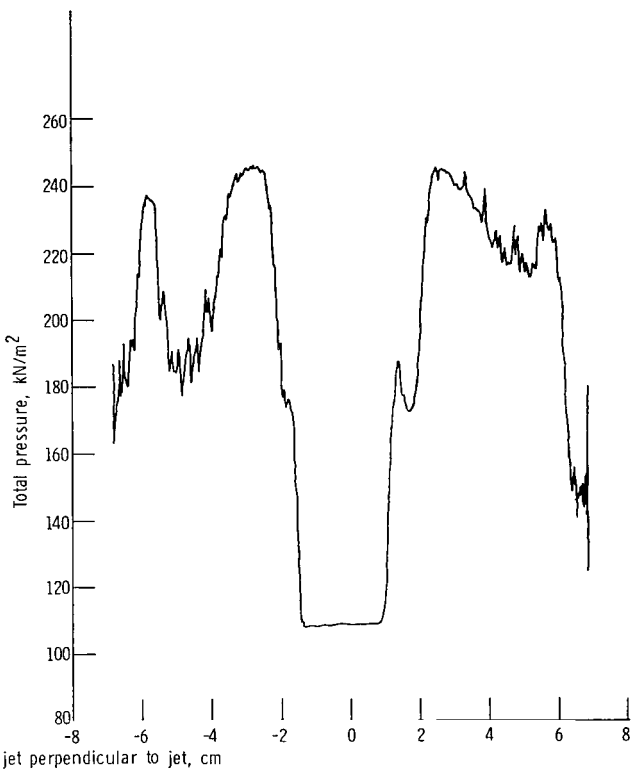

(d) Distance along plate from nozzle throat, x/D_t, 1.33.

Figure 17. - Continued.

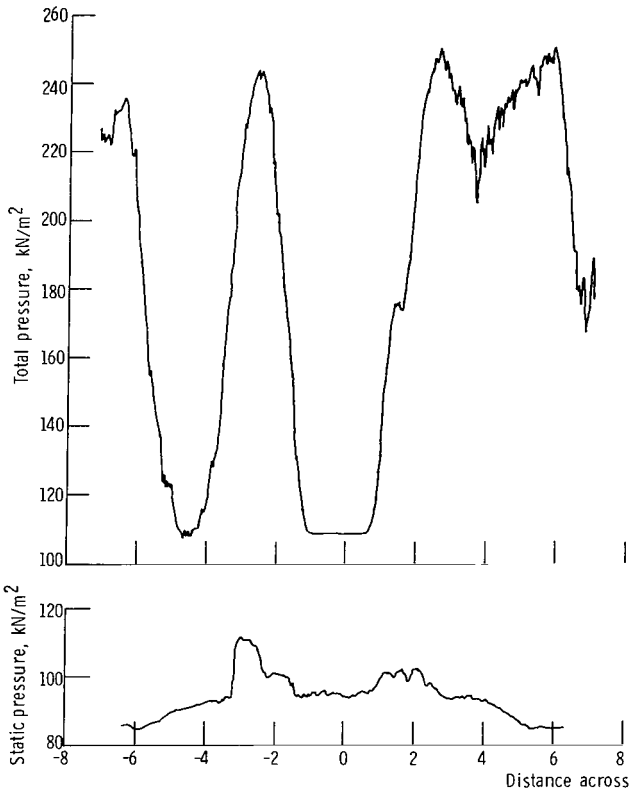

(e) Distance along plate from nozzle throat, x/D_t, 1.5.

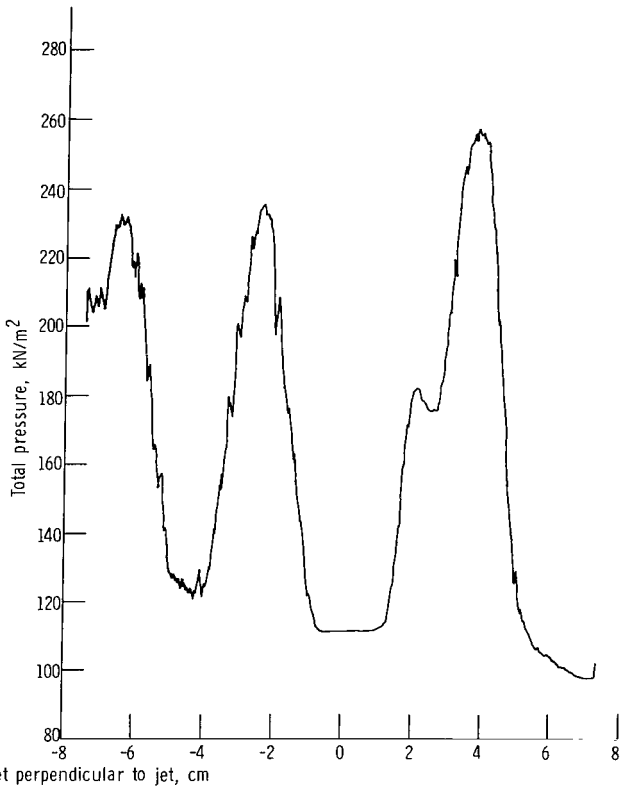

(f) Distance along plate from nozzle throat, x/D_t, 1.63.

Figure 17. - Continued.

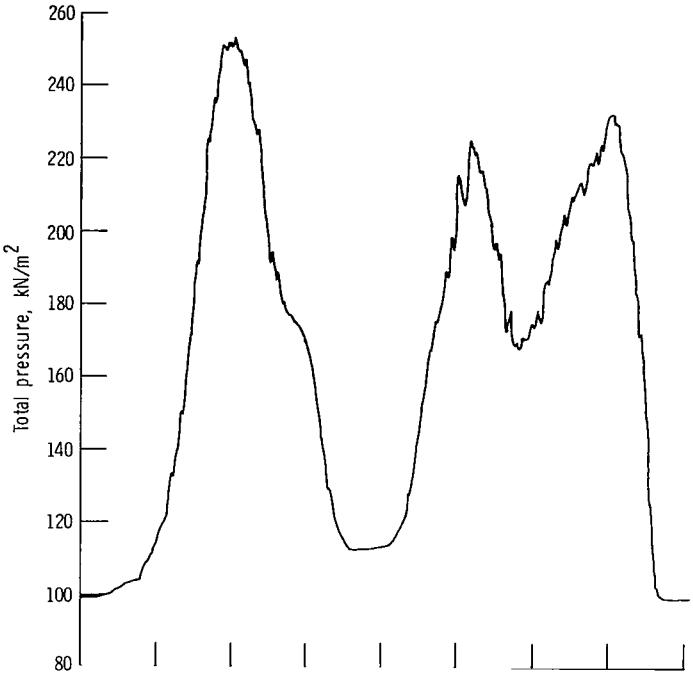

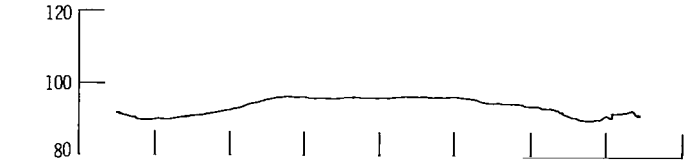

(g) Distance along plate from nozzle throat, x/D_t, 1.84.

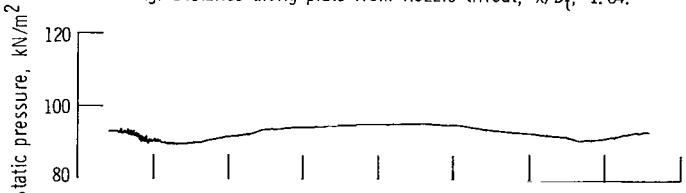

(h) Distance along plate from nozzle throat, x/D_t, 2.0.

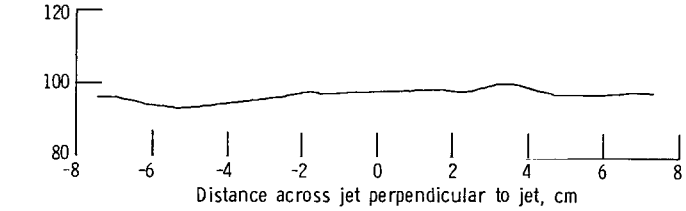

(i) Distance along plate from nozzle throat, x/D_t, 2.14.

Figure 17. - Continued.

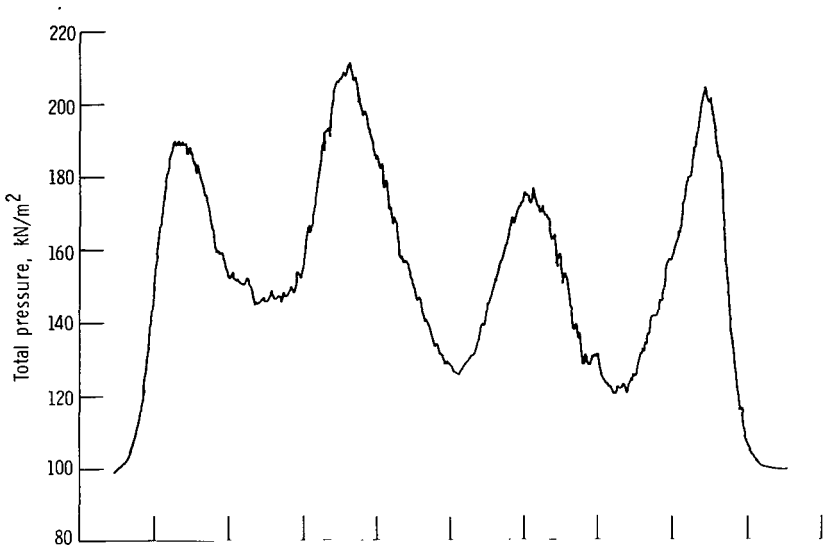

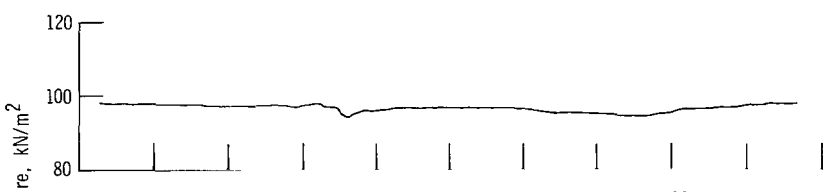

(j) Distance along plate from nozzle throat, x/D_t, 2.34.

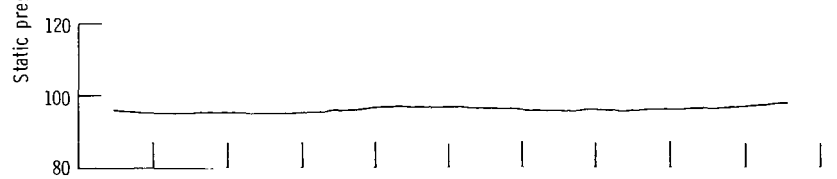

(k) Distance along plate from nozzle throat, x/D_t, 2.83.

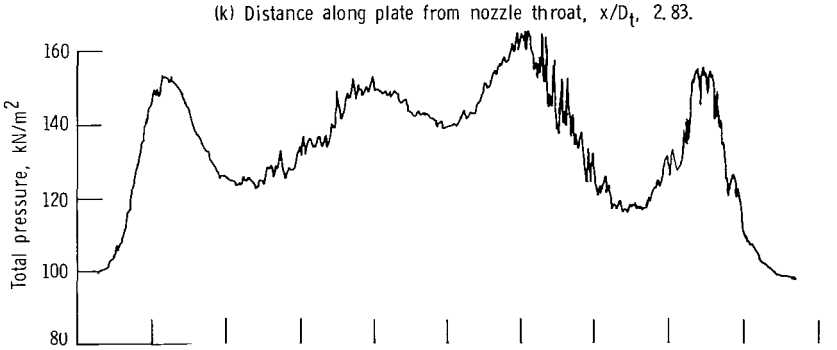

(l) Distance along plate from nozzle throat, x/D_t, 3.0.

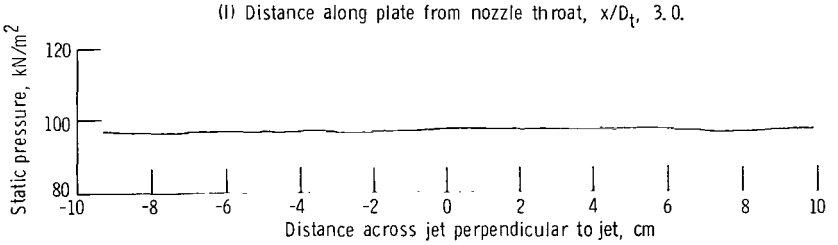

(m) Distance along plate from nozzle throat, x/D_t, 3.5.

Figure 17. - Continued.

(n) Distance along plate from nozzle throat, x/D_t, 4.0.

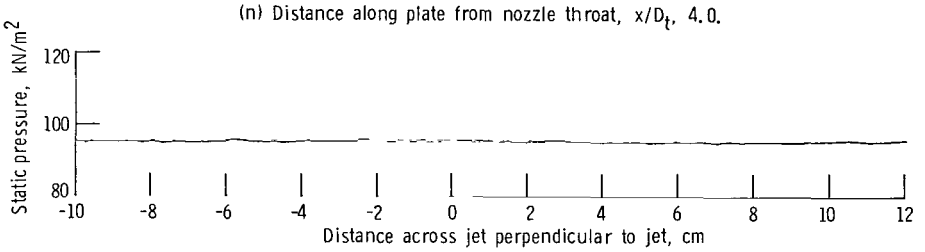

(o) Distance along plate from nozzle throat, x/D_t, 4.5.

Figure 17. - Concluded.

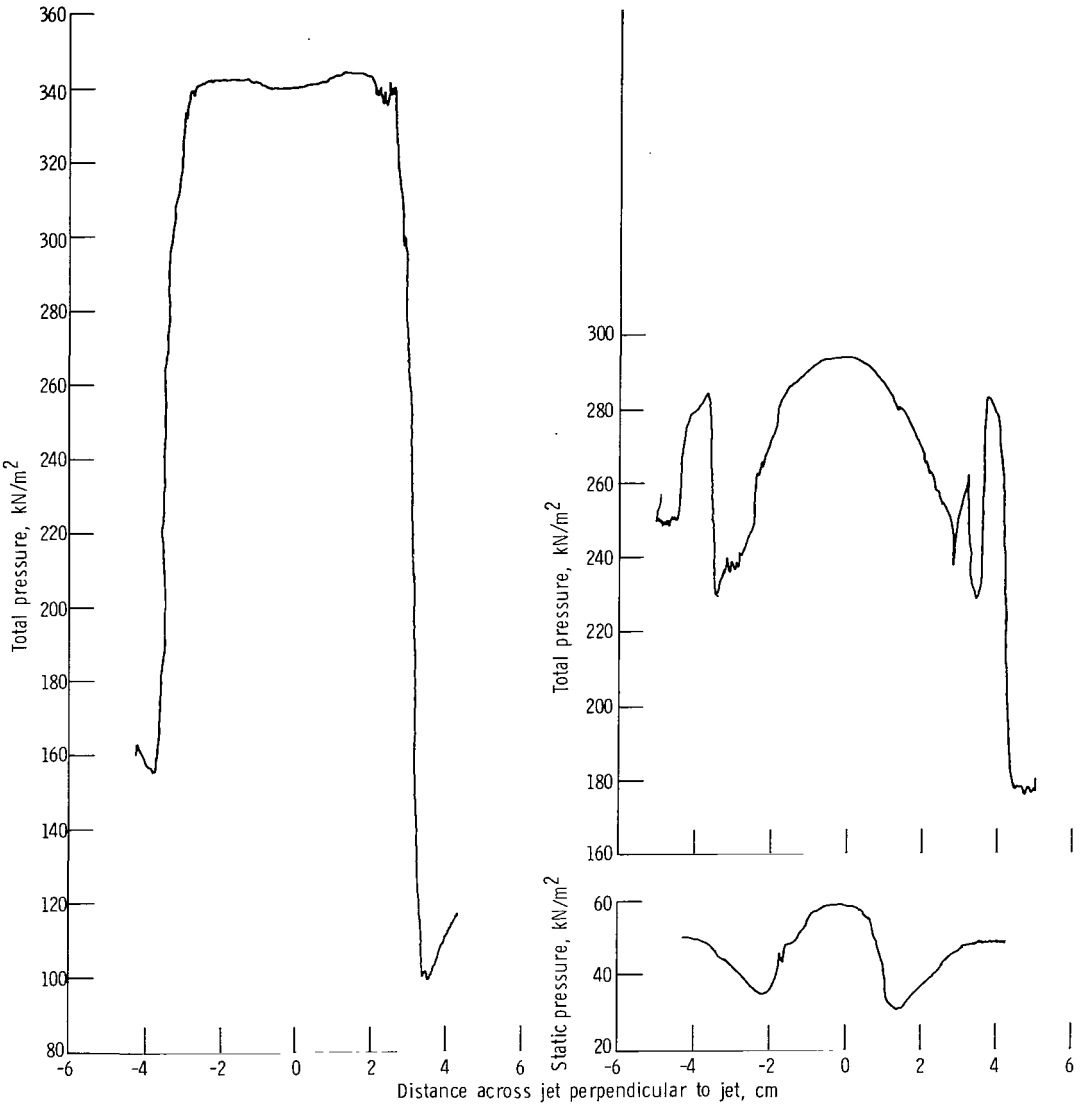

(a) Distance along plate from nozzle throat, x/D_t, 0.

(b) Distance along plate from nozzle throat, x/D_t, 0.5.

Figure 18. - Pitot and static pressure profiles perpendicular to nozzle centerline and through the center of opposing primary plates. Nozzle pressure ratio, 3.5.

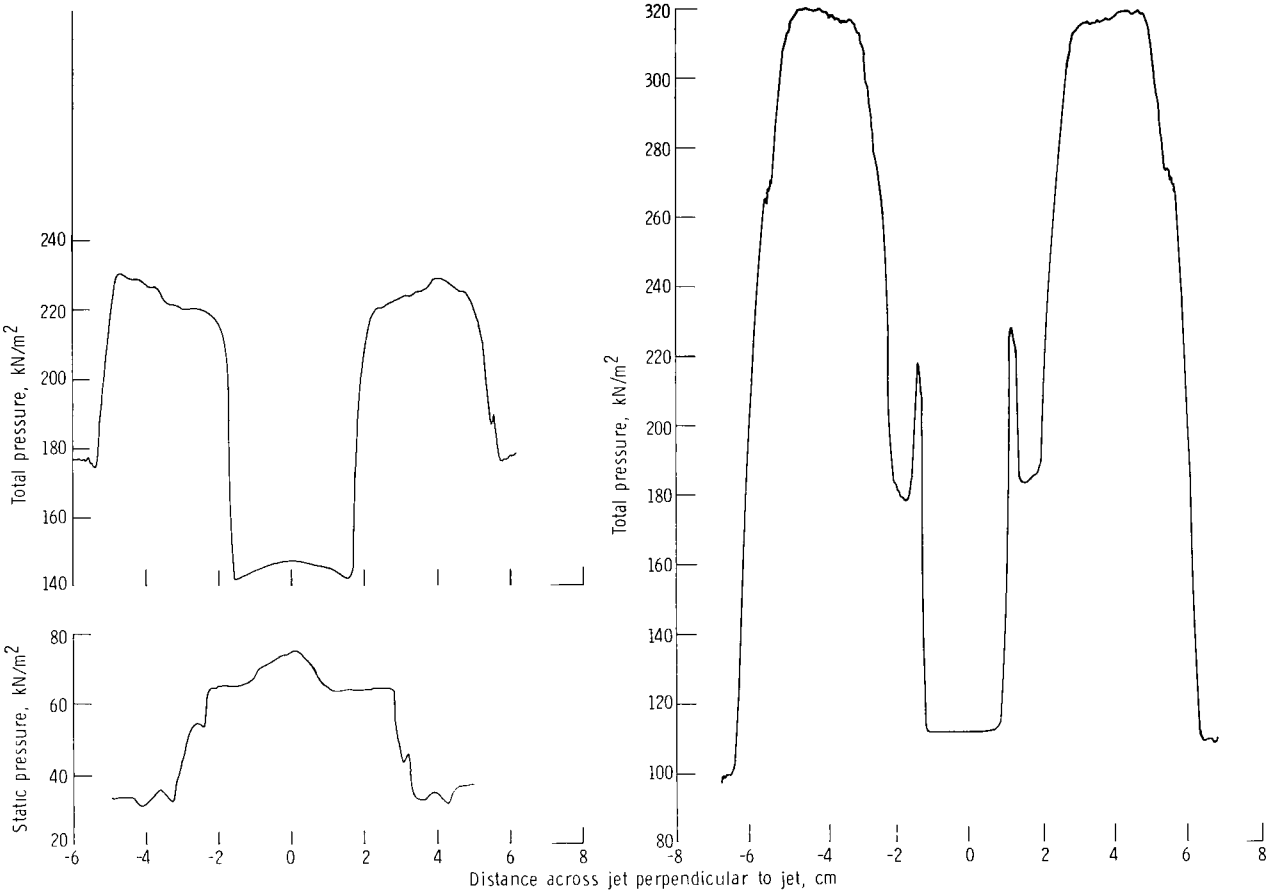

(c) Distance along plate from nozzle throat, x/D_t, 1.0.

(d) Distance along plate from nozzle throat, x/D_t, 1.33.

Figure 18. - Continued.

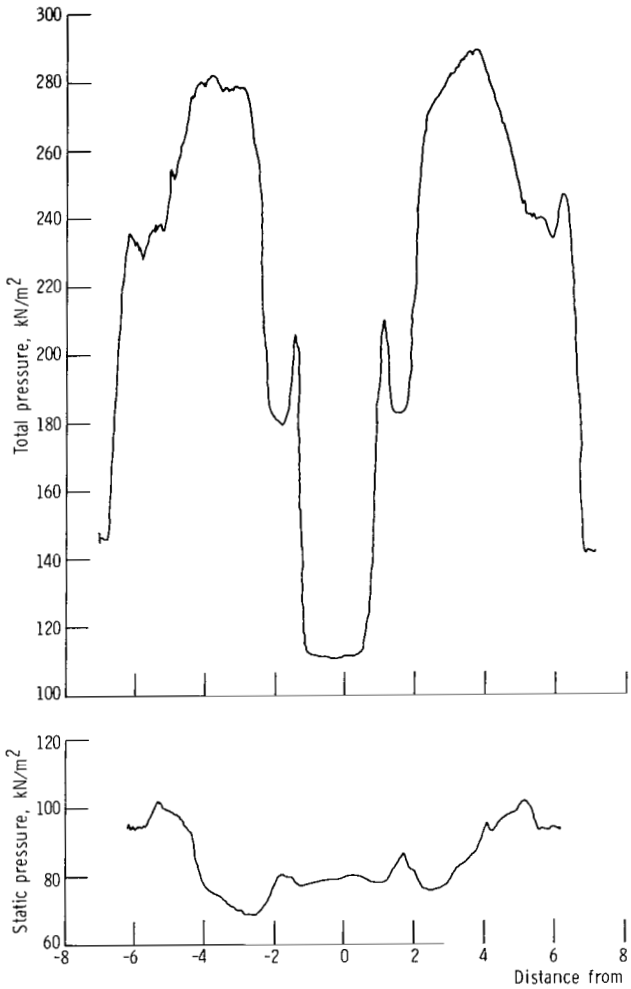

(e) Distance along plate from nozzle throat, x/D_t, 1.5.

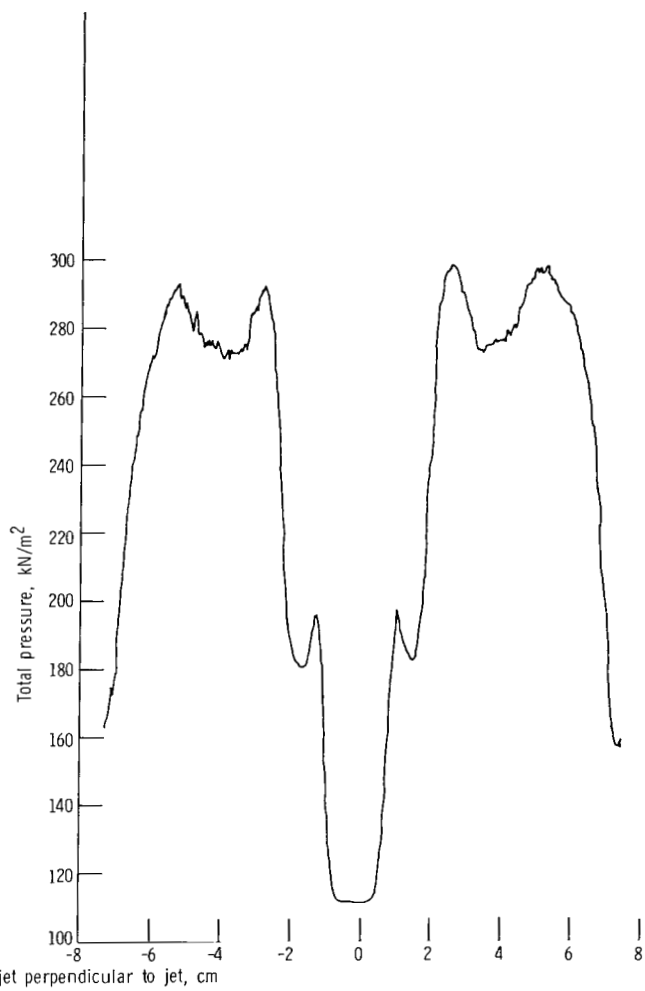

(f) Distance along plate from nozzle throat, x/D_t, 1.63.

Figure 18. - Continued.

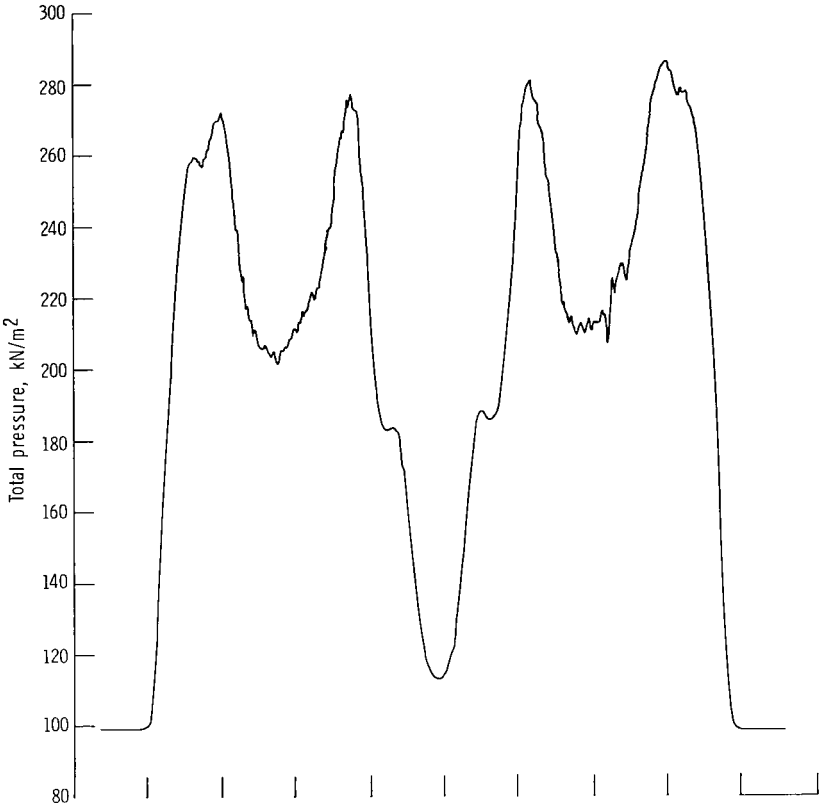

(g) Distance along plate from nozzle throat, x/D_t, 1.84.

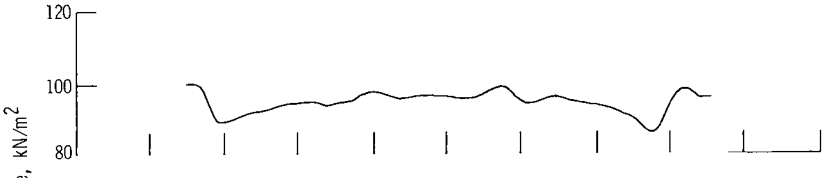

(h) Distance along plate from nozzle throat, x/D_t, 2.0.

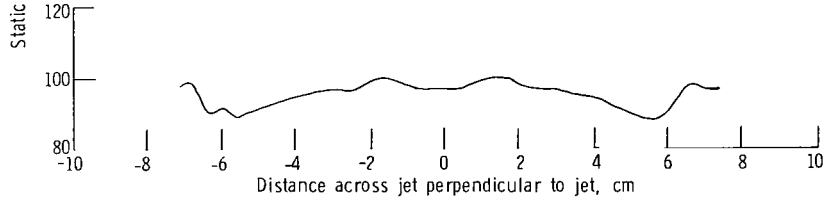

(i) Distance along plate from nozzle throat, x/D_t, 2.14.

Figure 18. - Continued.

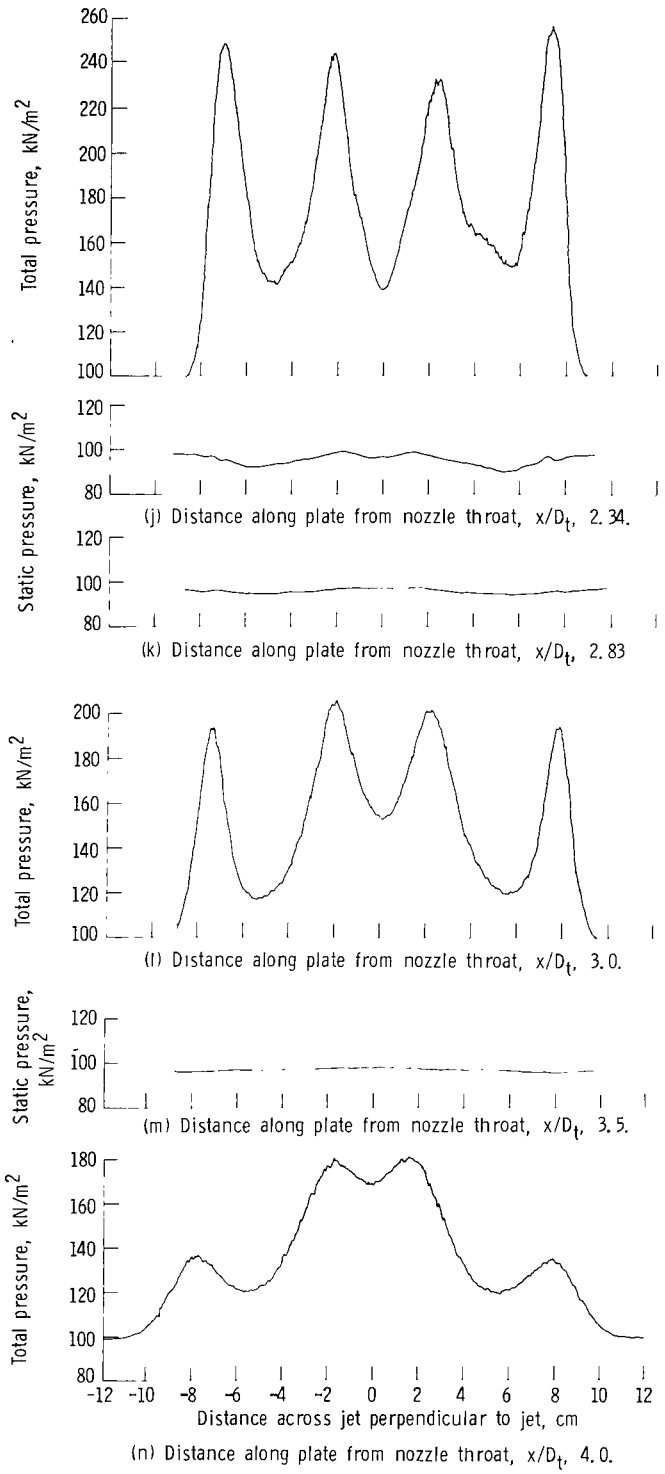

Figure 18. - Concluded.

NASA-Langley, 1972 —— 1 E-6640

"The aeronautical and space activities of the United States shall be conducted so as to contribute . . . to the expansion of human knowledge of phenomena in the atmosphere and space. The Administration shall provide for the widest practicable and appropriate dissemination of information concerning its activities and the results thereof."

—NATIONAL AERONAUTICS AND SPACE ACT OF 1958

NASA SCIENTIFIC AND TECHNICAL PUBLICATIONS

TECHNICAL REPORTS: Scientific and technical information considered important, complete, and a lasting contribution to existing knowledge.

TECHNICAL NOTES: Information less broad in scope but nevertheless of importance as a contribution to existing knowledge.

TECHNICAL MEMORANDUMS: Information receiving limited distribution because of preliminary data, security classification, or other reasons.

CONTRACTOR REPORTS: Scientific and technical information generated under a NASA contract or grant and considered an important contribution to existing knowledge.

TECHNICAL TRANSLATIONS: Information published in a foreign language considered to merit NASA distribution in English.

SPECIAL PUBLICATIONS: Information derived from or of value to NASA activities. Publications include conference proceedings, monographs, data compilations, handbooks, sourcebooks, and special bibliographies.

TECHNOLOGY UTILIZATION PUBLICATIONS: Information on technology used by NASA that may be of particular interest in commercial and other non-aerospace applications. Publications include Tech Briefs, Technology Utilization Reports and Technology Surveys.

Details on the availability of these publications may be obtained from:

SCIENTIFIC AND TECHNICAL INFORMATION OFFICE

NATIONAL AERONAUTICS AND SPACE ADMINISTRATION

Washington, D.C. 20546